

TSPulse: Dual Space Tiny Pre-Trained Models for Rapid Time-Series Analysis

Vijay Ekambaram, Subodh Kumar*, Arindam Jati*, Sumanta Mukherjee†, Tomoya Sakai†,
Pankaj Dayama, Wesley M. Gifford, Jayant Kalagnanam
IBM Research
vijaye12@in.ibm.com

Abstract

The rise of time-series pre-trained models has significantly advanced temporal representation learning, but current state-of-the-art models are often large-scale, requiring substantial compute. In this work, we introduce TSPulse, ultra-compact time-series pre-trained models with only 1M parameters, specialized to achieve strong performance across classification, anomaly detection, imputation, and retrieval tasks. TSPulse introduces innovations at both the architecture and task levels. At the architecture level, it employs a dual-space masked reconstruction strategy, learning from both time and frequency domains to capture complementary signal structures in a unified embedding space. This is further enhanced by a dual-embedding disentanglement approach, generating both detailed embeddings for fine-grained analysis and high-level semantic embeddings for broader task understanding. Notably, TSPulse’s semantic embeddings are designed to be robust to shifts in time, magnitude, and noise, which is fundamental for time-series semantic search. At the task level, TSPulse incorporates TSLens, a fine-tuning component that enables task-specific feature extraction for classification. It also introduces a multi-head triangulation mechanism, leveraging reconstruction deviations from multiple prediction heads, enhancing anomaly detection by fusing complementary model outputs. Additionally, a hybrid masking strategy improves zero-shot imputation by reducing pre-training mask bias. These architecture and task innovations collectively contribute to TSPulse’s significant performance improvements: 5-16% on the UEA classification benchmarks, +20% on the TSB-AD anomaly detection leaderboard, +50% in zero-shot imputation, and +25% in time-series retrieval. Remarkably, these results are achieved with just 1M parameters, making TSPulse 10-100x smaller than existing pre-trained models. Its efficiency enables GPU-free inference, rapid pre-training, and seamless task specialization, setting a new standard for efficient time-series pre-trained models. The models and source code are released under the Apache License and can be accessed from [here](#).

1 Introduction

Multivariate time-series (TS) analysis is crucial for various real-world applications, including forecasting, anomaly detection, imputation, classification, and retrieval. Transformer-based models such as PatchTST [24], Autoformer [38], and FEDFormer [43] have excelled at modeling long-range patterns but are computationally intensive. Lightweight alternatives like TSMixer [8] and TimeMixer [34] offer competitive accuracy with lower overhead, while self-supervised methods like TS2Vec [40], TNC [30], T-Rep [10], and BTSF [39] learn data-specific embeddings. However, these models typically require data-specific training and lack transferability.

*Equal second authorship. †Equal third authorship.

To address this, the TS community is embracing large-scale pre-training—mirroring trends in NLP and vision—enabling zero/few-shot generalization across tasks. Specialized models like TimesFM [5], Chronos [1], Moirai [36], and Lag-LLaMA [27] focus on forecasting, while general-purpose models like Moment [15] and UniTS [13] extend to imputation, classification, and anomaly detection. Meanwhile, cross-domain approaches such as Time-LLM [17], LLMTime [16], and GPT4TS [44] explore adapting large language models for time-series data.

Despite progress in TS pre-trained models, a key limitation remains: most are extremely large, with hundreds of millions or billions of parameters. This leads to high computational costs during deployment and tuning. Recent work like TTM [7] shows that compact models with 1–5M parameters can offer competitive zero/few-shot forecasting performance while staying efficient. However, such lightweight models are typically limited to forecasting and do not generalize to other tasks.

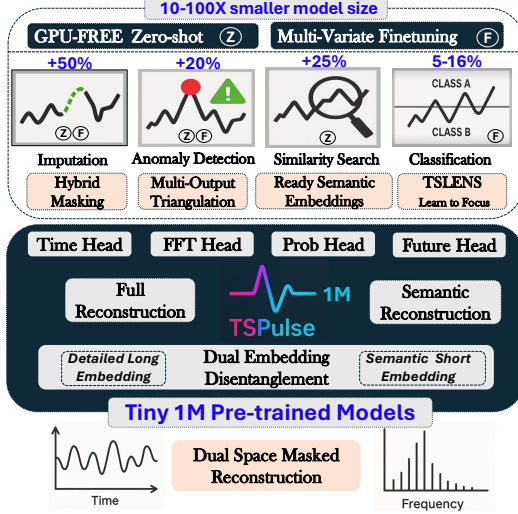


Figure 1: **TSPulse Overview.** % and X represent the accuracy and size improvements of TSPulse over SOTA pre-trained models across different benchmarks.

generates two types of embeddings during pre-training: (i) detailed embeddings for fine-grained analysis, and (ii) high-level semantic embeddings for broader task understanding. To achieve this, TSPulse performs masked reconstruction at two hierarchical levels: one targeting the full raw signal to capture detailed structures, and the other reconstructing a compact semantic signature to encode higher-level abstractions. These dual embeddings prove effective across diverse downstream tasks—some requiring semantic high-level cues (e.g., overall shape), others relying on low-level pattern fidelity (e.g., frequency distortions). By capturing both levels of information during pre-training, TSPulse enables faster and more robust generalization across tasks.

Building on the dual-embedding structure, we further introduce *TSLens*, a novel neural component that enables effective attention during fine-tuning by learning to focus on the most informative regions within and across the dual embeddings. This enables the model to prioritize task and data-relevant signals, enhancing performance while maintaining minimal computational overhead. Beyond fine-tuning, the same dual embedding design also proves highly effective for time-series zero-shot similarity search, as the compact semantic embeddings can be effectively used to retrieve time-series segments with similar patterns, even under real-world distortions like time shifts, magnitude changes, and noise. To our knowledge, TSPulse is the first model to offer GPU-free, out-of-the-box, ultra-compact semantic embeddings that are fast enough for real-time indexing.

In addition, TSPulse introduces a *hybrid masking pre-train strategy* that combines point-wise and block-wise masking with varying ratios per sample. This enables the model to reconstruct irregular masking structures, mimicking realistic scenarios. Unlike existing zero-shot imputation methods that are biased towards specific masking schemes (i.e. models trained with only block masking struggle on point-level gaps, and vice versa), TSPulse generalizes better across diverse missing data patterns.

Toward this, we introduce **TSPulse**, ultra-lightweight and versatile TS pre-trained models with just 1 million parameters, specialized to support a wide range of tasks such as anomaly detection, imputation, classification, and retrieval (Figure 1). Built on top of the lightweight TSMixer architecture, TSPulse introduces a set of novel design enhancements in both architecture and task workflows that significantly improve its performance. At the heart of TSPulse is a *dual-space masked reconstruction strategy*, in which masked inputs are simultaneously reconstructed in both time and frequency (FFT) domains. This joint learning leverages the intuition that certain patterns like sudden spikes are easier to detect in the time domain, while others such as periodicities, are more salient in the frequency domain. By learning to mix, attend and reconstruct across both spaces, TSPulse builds richer and robust representations.

Additionally, we introduce the concept of *dual-embedding disentanglement*, where TSPulse

Finally, TSPulse is pre-trained using a multi-objective loss that supervises multiple prediction heads—each responsible for reconstructing the input from the time domain, frequency domain, and producing a short-horizon forecast. This design is powerful and enables the model to detect deviations and anomalies from multiple complementary perspectives in an unsupervised way: sudden spike deviations may be evident in time, periodic shifts in frequency, and subtle drifts via forecast deviations. Through *multi-head triangulation*, TSPulse utilizes these complementary signals and achieves robust and reliable anomaly detection. Thus, TSPulse incorporates critical innovations at every stage in the standard masked reconstruction process that greatly enhances our performance in downstream tasks while keeping the model size extremely compact.

Contributions:

- **Compact & Versatile:** Ultra-compact pre-trained models (1M-parameters) with GPU-Free inference support and fast multivariate fine-tuning that can be specialized for a broad range of TS tasks—classification, imputation, anomaly detection (AD), and semantic search & retrieval.
- **Architectural Enhancers:** TSPulse introduces dual-space masked reconstruction paired with dual-embedding disentanglement, capturing complementary structures and also yielding ready-available fine-grained and high-level semantic embeddings.
- **Task Enhancers:** TSPulse introduces TSLens for task-aware embedding extraction, multi-head triangulation for cross-domain fusion for robust AD, hybrid masking for robust zero-shot irregular imputations, and tiny embeddings robust to shifts in time, magnitude and noise for similarity search.
- **Benchmarks:** With under 1M parameters, TSPulse outperforms models 10–100X larger—achieving 5–16% gains on UEA classification, +20% on TSB-AD benchmark/leaderboard (rank 1 in both uni- and multi-variate anomaly detection), +50% in zero-shot imputation, and +25% in TS similarity search task.
- **GPU-Free Zero-shot:** In addition to being highly efficient on GPUs, it provides near-instant zero-shot performance on CPUs.

2 TSPulse Architecture

Let $\mathbf{X} \in \mathbb{R}^{S \times C}$ denote a multivariate time-series with sequence length S and C channels. We begin by projecting and masking the data in both time and frequency domains. The resulting representations are processed by the backbone and decoder, which mix embeddings across all dimensions in both spaces. The learned embeddings are explicitly disentangled into two parts: the first is optimized via full reconstruction in both domains to capture *fine-grained features*, while the second, more compact part is trained using signature reconstruction to encode *global semantic representations*. These embeddings and outputs from the pre-trained model are then utilized by downstream tasks through various strategies. We now describe the core components of TSPulse, as illustrated in Figure 2.

Masking [Fig 2-①]: TSPulse begins with a *masking block* that hides portions of the input sequence to enable self-supervised reconstruction. Given an input $\mathbf{X} \in \mathbb{R}^{S \times C}$, we divide it into N non-overlapping patches of length pl and apply masking to obtain $\hat{\mathbf{X}} \in \mathbb{R}^{S \times C}$. TSPulse supports two masking strategies: **block masking** and **hybrid masking**. In block masking, entire patches are randomly replaced with a learnable mask token $\mathbf{M} \in \mathbb{R}^{1 \times pl}$, as commonly done in prior work [15, 13]. While effective for robust feature learning, this approach is inadequate for real-world imputation tasks, where missing values occur irregularly at both patch and point levels. To address this, we introduce a more realistic **hybrid masking** pre-train strategy that masks both full and partial patches within each sample using variable masking ratios, preventing overfitting to fixed patterns. A key design choice in TSPulse is to define the mask token $\mathbf{M} \in \mathbb{R}^{1 \times pl}$ at the *raw patch level*, unlike prior approaches that insert mask tokens in the embedding space [15, 32]. This enables individual time-points to be masked by selecting the appropriate value from \mathbf{M} based on their relative index within a patch (Figure 3(a)), allowing a single token to flexibly support both full and partial masking.

RevIN Normalization [Fig 2-②]: After masking, the masked time-series $\hat{\mathbf{X}}$ passes through a *Reversible Instance Normalization (RevIN)* block [18], which standardizes the unmasked portions to output $\mathbf{X}_m \in \mathbb{R}^{S \times C}$. Normalization statistics (mean and variance) are computed from the unmasked values, and scaling is applied to them with a learnable affine transformation.

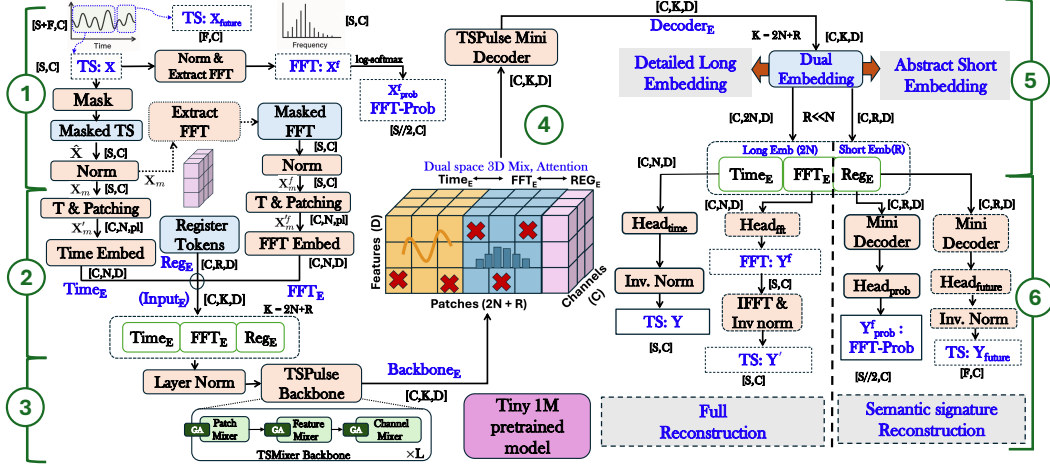


Figure 2: TSPulse Architecture. (X: Inputs, Y: Outputs, E: Embeddings). Annotations for easy reference: ①-⑥.

FFT Extraction [Fig 2-①]: As TSPulse reconstructs in both time and frequency domains, this block extracts masked FFT features for backbone processing and also prepares the corresponding ground-truth for loss computation. Instead of explicitly masking the frequency space, we feed the scaled and masked time-series X_m directly into the Fast Fourier Transform (`torch.fft.rfft`) [26], propagating the mask and ensuring the same data is consistently hidden in both spaces, preventing leaks. The real and imaginary FFT outputs from X_m are then packaged, scaled, and processed into tensor $X_m^f \in \mathbb{R}^{S \times C}$ for further backbone processing. Refer to Appendix. A.7 for more details.

Simultaneously, two ground-truths are computed from the frequency representation. First, the unmasked scaled time-series is transformed using the same approach described above to get $X^f \in \mathbb{R}^{S \times C}$, a clean, unaltered frequency representation of the time-series, which is used to guide the model’s reconstruction. In addition, we also compute the log-magnitude spectrum of the unmasked time-series and apply softmax to obtain $X_{\text{prob}}^f \in \mathbb{R}^{S/2 \times C}$, a normalized global frequency signature (Appendix. A.7 for more details). This global signature serves as an auxiliary reconstruction target, helping the model capture high-level semantic patterns and improving generalization to downstream tasks. The log transformation reduces the dynamic range and stabilizes training, while softmax emphasizes dominant spectral components, mapping the output to a probability-like distribution.

Encoding [Fig 2-②]: This block projects the input to an embedding space. The masked time-domain input $X_m \in \mathbb{R}^{S \times C}$ is transposed and then divided into N non-overlapping patches of length pl , resulting in a tensor of shape $\mathbb{R}^{C \times N \times pl}$. Note that the same patch length was used during masking. Now, each patch is projected via a linear layer from $\mathbb{R}^{pl} \rightarrow \mathbb{R}^D$ to obtain time-encoded features $\text{Time}_E \in \mathbb{R}^{C \times N \times D}$. Similarly, the masked frequency-domain input $X_m^f \in \mathbb{R}^{S \times C}$ is transposed, patched and projected to produce frequency-encoded features $\text{FFT}_E \in \mathbb{R}^{C \times N \times D}$. Motivated by recent advances in vision transformers [4], where adding learnable register tokens stabilizes training and improves transfer learning, we introduce R such tokens shared across channels: $\text{Reg}_E \in \mathbb{R}^{C \times R \times D}$. The full input to the backbone is constructed by concatenating time, frequency, and register tokens along the patch axis and layer normalized: $\text{Input}_E = [\text{Time}_E; \text{FFT}_E; \text{Reg}_E] \in \mathbb{R}^{C \times (2N+R) \times D} = \mathbb{R}^{C \times K \times D}$.

TSPulse Backbone [Fig 2 - ③,④]: The TSPulse backbone receives $\text{Input}_E \in \mathbb{R}^{C \times K \times D}$, a unified sequence of masked patches from both time and frequency domains, along with learnable register tokens. Its goal is to transform this input into semantically rich, task-robust representations. To maintain efficiency, we use the *TSMixer* backbone [8], an MLP-Mixer based alternative to Transformers that performs strongly with reduced compute [7]. *TSMixer* has stacked Mixer blocks interleaved with lightweight gated attention, enabling flexible feature mixing across three dimensions: within-patch, across-patch, and across channels. Since Input_E already integrates both time and frequency information, *TSMixer* effectively fuses these views, learning *dual-space representations* that capture temporal and spectral correlations. Gated attention [8] further prioritizes informative regions, enhancing the model’s ability to generalize across downstream tasks.

TSPulse Mini-Decoder [Fig 2-④]: The backbone output ($\text{Backbone}_E \in \mathbb{R}^{C \times K \times D}$) is passed through a lightweight *mini-decoder*, which mirrors the backbone but is only 10–20% of its size. This compact decoder refines and adapts learned representations during fine-tuning, enabling efficient task-specific decoding with minimal computational overhead, ensuring fast adaptation while preserving pre-training efficiency and generalization.

Multi-Objective Heads [Fig 2-⑤]: The output of the decoder, denoted as $\text{Decoder}_E \in \mathbb{R}^{C \times (2N+R) \times D}$, is disentangled into distinct embedding types, each optimized for a different reconstruction objective. TSPulse introduces *dual-embedding disentanglement* which creates principled separation between (1) *long embeddings* for full reconstruction and (2) *short embeddings* for high-level semantic tasks. The first $2N$ patch embeddings correspond to the time and frequency domains and capture fine-grained temporal and spectral patterns. These are used for *detailed reconstruction*. In contrast, the final R register embeddings—compact and abstract by design—are self-supervised to summarize global structure and are used for *semantic reconstruction* tasks such as short-horizon forecasting and global frequency signature prediction. This dual-embedding design ensures that both low-level fidelity and high-level semantics are jointly modeled.

- **Reconstruction Heads [Fig 2-⑥]:** The first N patch embeddings from Decoder_E pass through a linear layer (Time Head) and inverse RevIN to obtain the reconstruction \mathbf{Y} of the input time-series. The next N embeddings from the decoder are projected (via the FFT Head) to reconstruct the input frequency spectrum \mathbf{Y}^f , which is further reshaped, passed through `torch.iff`, and inverse RevIN to yield \mathbf{Y}' , an alternate reconstruction of the input time-series from FFT-space. Losses are computed as Mean Squared Errors (MSE): $\mathcal{L}_{\text{time1}} = \text{MSE}(\mathbf{X}, \mathbf{Y})$, $\mathcal{L}_{\text{time2}} = \text{MSE}(\mathbf{X}, \mathbf{Y}')$, and $\mathcal{L}_{\text{fit}} = \text{MSE}(\mathbf{X}^f, \mathbf{Y}^f)$, where the first two losses are computed only on the masked time-points.
- **Semantic Heads [Fig 2-⑥]:** The final R register embeddings from Decoder_E pass through different heads for high-level semantic reconstructions. One head outputs $\mathbf{Y}_{\text{prob}}^f$, a predicted softmax distribution over the log-magnitude frequency spectrum, trained with cross-entropy loss $\mathcal{L}_{\text{prob}} = \text{CE}(\mathbf{X}_{\text{prob}}^f, \mathbf{Y}_{\text{prob}}^f)$ to capture global spectral semantics. A second head predicts a short-horizon forecast $\mathbf{Y}_{\text{future}}$, trained with MSE loss $\mathcal{L}_{\text{future}} = \text{MSE}(\mathbf{X}_{\text{future}}, \mathbf{Y}_{\text{future}})$ to model high-level temporal dynamics. Unlike traditional forecasting, the goal is not long-range prediction but improving the semantic richness of the embeddings for downstream tasks. Importantly, each semantic head is paired with a lightweight decoder, ensuring task-agnostic register embeddings without overfitting.

Finally, a weighted sum of all the above losses is jointly minimized during pre-training. This multi-headed architecture—anchored in the dual-embedding formulation—enables TSPulse to learn both fine-grained reconstructions and compact, high-level semantic embeddings, making it highly transferable across a diverse range of time-series tasks.

3 TSPulse Workflows

Pre-training: TSPulse is pre-trained on diverse $\sim 1\text{B}$ TS samples as detailed in Appendix A.5. Inspired by the success of small, task-specialized pre-trained models in the language/vision domain [28][23][12][19]—which achieve strong performance through minimal task-specific adaptations—we extend this strategy to time-series. Specifically, we specialize the pre-training for every task through reweighting loss objectives to prioritize heads most relevant to the target task. This enables TSPulse to refine task-specific representations while maintaining its lightweight design, facilitating efficient transfer learning across any datasets for the specified downstream task. Refer Appendix A.6 for more details. Pre-training on 1B samples takes just one day with $8 \times \text{A100}$ GPUs, thus there are no practical challenges in pre-training task-specific models.

In addition, given the heterogeneous channel counts in pre-training datasets, TSPulse is pre-trained in a univariate mode ($c = 1$), treating each channel independently. Cross-channel modeling is deferred to fine-tuning, where channel-mixing is selectively activated based on the target dataset [7].

Target data Fine-Tuning: During fine-tuning, the pre-trained model—already strong in zero-shot settings—is further adapted to the target data by updating the decoder and task-specific heads. For multivariate inputs, we enable *channel mixing* in the decoder to capture inter-channel correlations, which are absent in the univariate pre-training setup. Our design draws inspiration from TTM [7],

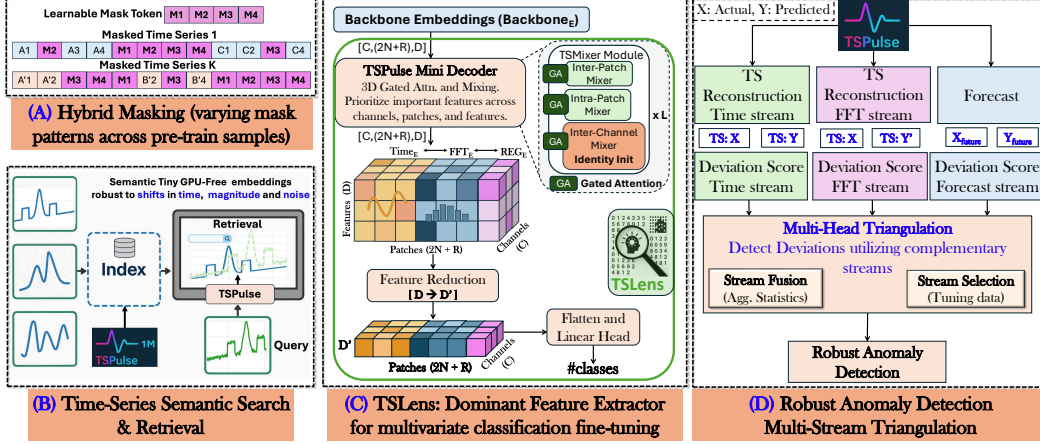


Figure 3: TSPulse Downstream Differentiators.

where channel mixer blocks are interleaved between patch and feature mixers within each TSMixer layer. A key limitation in the original design is the *random initialization* of these mixers, which introduces untrained parameters between already pre-trained layers. This can disrupt information flow and create sharp activation shifts, leading to unstable gradient propagation, especially during the early stages of fine-tuning. To address this, we initialize channel mixers with *identity weights*, which enable smooth gradient flow between pre-trained weights. These layers gradually learn inter-channel dependencies without interfering with earlier knowledge, leading to a significantly more stable fine-tuning process, as confirmed by our experiments.

Downstream Tasks: TSPulse delivers strong zero-shot performance for tasks like *imputation* and *semantic search* by directly leveraging its reconstructions and embeddings. Hybrid masked pre-training (Fig. 3-A) enhances imputation robustness, while register token embeddings enable resilient similarity search under time, magnitude, and noise shifts (Fig. 3-B). For *classification* and *anomaly detection*, TSPulse incorporates task-specific innovations, detailed below.

Classification via TSLens: TSPulse supports classification through a lightweight fine-tuning module, **TSLens** (Fig. 3-C), which replaces standard pooling with a learned mechanism that adaptively extracts relevant features from dual embeddings. Unlike conventional methods, which average or max-pool all patch-level embeddings followed by a linear head, TSLens selectively attends to and weights features across fine-grained patch embeddings and high-level register tokens.

TSLens takes the backbone output $\text{Backbone}_E \in \mathbb{R}^{C \times (2N+R) \times D}$, passes it through the mini decoder (initialized with pre-trained weights and channel-mixing enabled), and learns cross-channel dependencies via identity-initialized channel mixers as explained in Section 3. The resulting representation $\mathbf{H} \in \mathbb{R}^{C \times (2N+R) \times D}$ is projected to a lower-dimensional space $\mathbf{H}' \in \mathbb{R}^{C \times (2N+R) \times D'}$, flattened into $\mathbf{H}_{\text{flat}} \in \mathbb{R}^{C \cdot (2N+R) \cdot D'}$, and passed through a linear layer to produce class logits $\mathbf{y}_{\text{pred}} \in \mathbb{R}^{\text{num_classes}}$. The model is optimized with cross-entropy loss. This design allows TSPulse to dynamically focus on the most informative features across local and global representations, improving classification accuracy across diverse datasets.

Robust Anomaly Detection via Multi-Head Triangulation: In Anomaly Detection, we observe that some anomalies are easily detectable in the time domain (e.g., sudden spikes), others in the frequency domain (e.g., periodicity disruptions), and still others through future forecasts (e.g., missing trends). Since TSPulse offers multi-prediction heads—the time reconstruction head ($\text{Head}_{\text{time}}$), the frequency reconstruction head (Head_{fft}), and the short-horizon forecasting head ($\text{Head}_{\text{future}}$)—each head learns to reconstruct or forecast the time-series from a different perspective, capturing fine-grained signal continuity, spectral consistency, and predictive temporal dynamics, respectively. This enables TSPulse to detect a diverse range of anomalies.

During inference, anomaly scores are computed from each head based on the deviations between the original and predicted signals (Fig. 3-D). Once the deviations are obtained from all heads, two approaches are possible. **Approach 1** ($\text{Head}_{\text{ensemble}}$) is to fuse the normalized scores using statistics,

such as the maximum, to generate a unified score. In **Approach 2** ($\text{Head}_{\text{triang.}}$), when a small labeled validation set is available, it can be used to select the most effective head in zero-shot from the above four heads (including $\text{Head}_{\text{ensemble}}$). This allows the model to adapt to the anomaly type and structure specific to each application. Notably, TSPulse is the first pre-trained model to unify and triangulate multi-space outputs in a single lightweight framework, enabling robust anomaly detection in both zero-shot and fine-tuned settings.

4 Experiments

We evaluate TSPulse across 4 downstream tasks: classification, anomaly detection, imputation, and similarity search. Details of the pre-trained model configurations are in Appendix A.6. Pre-training datasets are listed in Section 4, and they do not overlap with any of the evaluation datasets.

4.1 Anomaly Detection (AD)

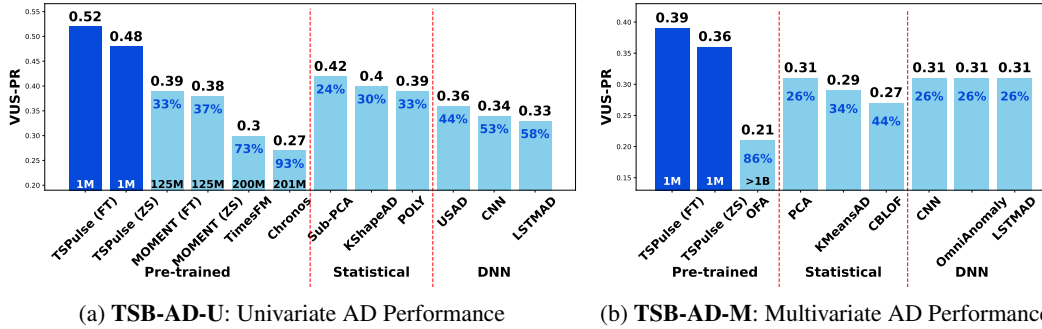


Figure 4: VUS-PR (official metric, higher is better) scores of different AD methods on the TSB-AD leaderboard; **IMP(%)**—the percentage improvement of TSPulse over baselines; A maximum of top three SOTA models have been reported in each category. Full results across all 40 models are in Appendix A.8.

Setup: We evaluate TSPulse on the TSB-AD benchmark [20] (recent and comprehensive leaderboard for AD), which comprises 40 eval datasets, covering both univariate (TSB-AD-U) and multivariate (TSB-AD-M) anomaly detection. The benchmark includes results from 40 SOTA methods and establishes VUS-PR [25] as the primary and robust evaluation metric. A small labeled official *tuning-set* is provided for hyperparameter selection, consistently used across all leaderboard methods. We adopt this tuning set for multi-head triangulation to select the best-performing head and report scores on the test set for both zero-shot (TSPulse-ZS) and fine-tuned (TSPulse-FT) variants. In the zero-shot case, TSPulse is evaluated directly without training on the target data; in the fine-tuned case, it is self-supervised using the official training split without access to any anomaly labels. Note that all non-pretrained neural network models are also trained using the same training split. Figure 4 summarizes VUS-PR results. Full details are in Appendix A.8.

Results: As illustrated in Figure 4, TSPulse (ZS) outperforms all existing SOTA methods on both the univariate and multivariate anomaly detection benchmarks. Specifically, TSPulse (ZS) achieves 14% and 16% higher VUS-PR scores compared to the best-performing baselines—SubPCA for the univariate setting and CNN for the multivariate setting, respectively. Notably, TSPulse, without any training on the target data, outperforms all models trained on it, underscoring its strong transfer learning. TSPulse also outperforms all the pre-trained models by +30% by using just a fraction of their model size.

The fine-tuned variant, TSPulse (FT), further improves results, achieving 24% and 26% gains over SOTA on univariate and multivariate benchmarks, respectively. These results underscore the effectiveness of TSPulse for diverse anomaly detection tasks.

4.2 Classification

Setup: We evaluate TSPulse results on 29 datasets from the UEA Multivariate Time Series Classification Archive [2]. Dataset and hyperparameter details are provided in Appendix A.9.

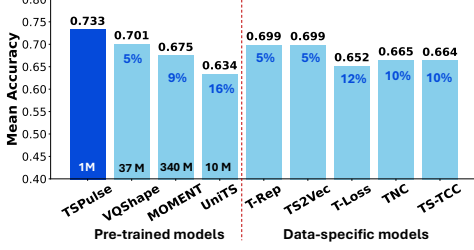


Figure 5: Classification Mean Accuracy results (higher is better); **IMP(%)**—the percentage improvement of TSPulse over baselines.

We compare against recent pre-trained models—VQShape [35], Moment [15], and UniTS [13]—as well as strong data-specific baselines including T-Rep [10], TS2Vec [40], T-Loss [11], TS-TCC [9] and TNC [30].

Results Classification results fine-tuned/trained on the labeled data are reported in Figure 5. TSPulse achieves state-of-the-art accuracy, surpassing VQShape, UniTS, and Moment by 5–16%, while being drastically smaller (1M vs. 10–340M parameters). It also outperforms contrastive and supervised baselines by 5–12%, highlighting the effectiveness of TSPulse fine-tuning with TSLens.

4.3 Imputation

Setup: We evaluate TSPulse on 6 LTSF benchmark datasets [38]: ETTh1, ETTh2, ETTm1, ETTm2, Weather, and Electricity, under 4 mask ratios (12.5%, 25%, 37.5%, 50%) using *irregular hybrid masking* (a mix of block and point-level masks) to simulate real-world missingness.

Results: We first evaluate TSPulse in a fully Zero-Shot (ZS) setup, requiring no data-specific tuning. Among pre-trained baselines, MOMENT supports native zero-shot imputation, for UniTS [13] the pretrained model is prompt-tuned (PMT) with 10%

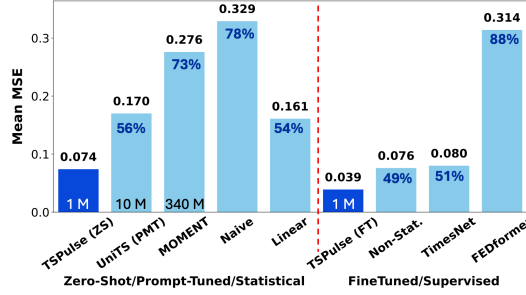


Figure 6: Hybrid Masking imputation MSE results (Lower is better). **IMP(%)**—the percentage improvement of TSPulse over baselines.

data in multi-task setup. We also compare against statistical baselines in ZS setup. As shown in Figure 6, TSPulse (ZS) outperforms MOMENT by over 70% and UniTS by 50% despite its prompt-tuning. Compared to statistical interpolation methods, TSPulse shows 50%+ gains, highlighting the effectiveness of TSPulse in hybrid masking setup and robust zero-shot generalization. More details in Appendix A.10

When Fine-Tuning (FT) is desired, TSPulse can be extended with a channel-mixing decoder to capture inter-variable dependencies, outperforming strong supervised models like Times-

4.4 Time-Series Similarity Search & Retrieval

Setup: We evaluate TSPulse’s similarity search using its *short register embeddings* (i.e zero-shot semantic embeddings) to retrieve time-series segments with similar patterns, even under real-world distortions like time shifts, magnitude changes, and noise. Since time-series are typically indexed via high-stride sliding windows for efficient storage, the same pattern can appear in different positions, making distortion-invariant embeddings essential for similarity search. We use real and synthetic data for indexing, and generate query samples by applying complex augmentations (time shifts, magnitude changes, and noise distortions) from indexed samples. This setup tests the embeddings’ robustness in retrieving distorted similar patterns and simplifies evaluation, as the correct matches for each query are already known. Two tasks are defined: *Family Match* for high-level pattern retrieval and *Fine-Grained Match* for precise pattern matching and evaluated using PREC@k and MRR@k [31]. We construct a synthetic dataset and a real dataset based on the UCR dataset [3], and report the average score across both for each task. See Appendix A.11 for full details.

Results: Figure 7 compares TSPulse’s similarity search performance against zero-shot embeddings from MOMENT and Chronos. We use their smallest variants to closely match TSPulse’s embedding

size and enable faster indexing for a fair comparison. As shown, TSPulse outperforms MOMENT by over 25% in family-level and 40% in fine-grained match accuracy, and surpasses Chronos by 100%. Notably, TSPulse’s zero-shot embeddings are 2X smaller and enable 10–100X faster CPU inference, 9–15X faster GPU inference, and come from a model that is 40× smaller than the baselines. Further discussion in Appendix A.11.

Embedding Analysis: We analyze the sensitivity of embeddings to various input perturbations as explained in Appendix A.12. Embeddings remain robust and relatively insensitive to distortions such as noise, magnitude shifts, time shifts, and missingness. In contrast, changes in frequency and underlying patterns are more prominently reflected in the embedding space. This desirable property—being highly sensitive to semantic structure and patterns while remaining resilient to distortions and temporal shifts—greatly enhances similarity search performance.

5 Ablation studies

Anomaly Detection (AD) We evaluate the performance of individual TSPulse heads for anomaly detection. Table 1(a) reports average VUS-PR scores for each head used independently. The proposed multi-head triangulation outperforms all single-head variants on both TSB-AD-U and TSB-AD-M, demonstrating the strength of multi-head TSPulse. See Appendix A.8 for details.

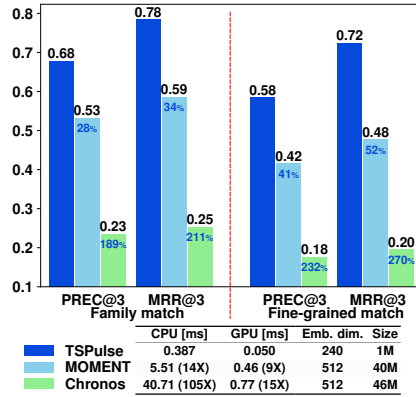


Figure 7: Similarity Search results using zero-shot embeddings (Higher is better). IMP(%)—the percentage improvement of TSPulse over baselines.

(i.e., w/o Hybrid PT), performance drops by 79% under hybrid-mask eval settings, underscoring the importance of hybrid masking in pre-training for robust, generalizable imputation, where missingness is irregular and more reflective of real-world scenarios.

Similarity Search Table 1(d) shows that TSPulse and baselines perform similarly without distortion. As augmentation distortion increases, all models degrade, but TSPulse remains notably more robust to time shifts, magnitude changes, and noise—highlighting the resilience of its embeddings in retrieving distorted yet similar patterns.

Efficiency: Appendix A.13 shows TSPulse is significantly faster, smaller and CPU-friendly.

6 Conclusion

TSPulse sets a new benchmark for ultra-compact time-series pre-trained models, achieving state-of-the-art performance in classification, imputation, anomaly detection, and similarity search—all with under 1M parameters. Powered by innovations like dual-space reconstruction, disentangled

Classification We evaluate the impact of key design components in Table 1(b), using a representative subset of 17 UEA datasets for faster analysis. Removing either the short or long embedding from the *dual-embedding* design reduces mean accuracy by 8–10%, confirming the importance of capturing both semantic and fine-grained features. Disabling *masking* during fine-tuning leads to an 8% drop—especially on smaller datasets—highlighting its role as a regularizer. Replacing *TSLens* with simple pooling causes an 11–16% drop, emphasizing the value of feature-attention. Randomly initializing the *channel-mixing (CM)* blocks instead of using identity weights leads to a 9% drop, reflecting the need for stable gradient flow. Removing *dual-space learning* (i.e., reconstructing only in time domain) lowers accuracy by 7%, and omitting *virtual channel expansion*, critical for low-channel datasets—causes a further 2% drop. More details in Appendix 12.

Imputation Table 1(c) shows that removing dual-space reconstruction leads to an 8% drop in zero-shot accuracy. When pre-training (PT) is done with only block masking

Variate	TSPulse Head	VUS-PR
Uni.	Head_{triang.}	0.48
	Head _{ensemble}	0.44 9% ↓
	Head _{time}	0.42 14% ↓
	Head _{fft}	0.42 14% ↓
	Head _{future}	0.30 60% ↓
Multi.	Head_{triang.}	0.36
	Head _{ensemble}	0.31 16% ↓
	Head _{time}	0.31 16% ↓
	Head _{fft}	0.31 16% ↓
	Head _{future}	0.24 50% ↓

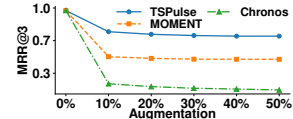
(a) Zero-shot Anomaly Detection

Model Variant	Accuracy
TSPulse	0.747
w/o Short Embedding	0.689 8% ↓
w/o Long Embedding	0.681 10% ↓
w/o Mask	0.691 8% ↓
w/o CM Identity Init	0.685 9% ↓
w/o Channel Expansion	0.734 2% ↓
w/o TSLens (Avg-Pool)	0.675 11% ↓
w/o TSLens (Max-Pool)	0.645 16% ↓
w/o Dual-space Learning	0.696 7% ↓

(b) Classification Accuracy

Model Variant	MSE
TSPulse	0.074
w/o Dual-Space	0.081 8% ↓
w/o Hybrid PT	0.354 79% ↓

(c) Imputation MSE



(d) Similarity Search

Table 1: Ablation results across tasks. [VUS-PR, Accuracy, MRR]: Higher is better; [MSE]: Lower is better. IMP(%) indicates the percentage improvement of the bold variant over the compared variant.

embeddings, TSLens, hybrid masking, and multi-head triangulation, TSPulse enables robust zero-shot and fine-tuned performance. Despite its small size, it outperforms models 10–100X larger and runs efficiently on CPUs, making it both powerful and deployment-ready. Appendix A.14 outlines limitations and future directions, including opportunities to expand to additional downstream tasks, enable incremental learning and reduce supervision requirements. We believe this work will inspire more advanced research and innovation in the field of lightweight time-series modeling.

References

- [1] Abdul Fatir Ansari, Lorenzo Stella, Caner Turkmen, Xiyuan Zhang, Pedro Mercado, Huibin Shen, Oleksandr Shchur, Syama Sundar Rangapuram, Sebastian Pineda Arango, Shubham Kapoor, et al. Chronos: Learning the language of time series. *arXiv preprint arXiv:2403.07815*, 2024.
- [2] Anthony Bagnall, Hoang Anh Dau, Jason Lines, Michael Flynn, James Large, Aaron Bostrom, Paul Southam, and Eamonn Keogh. The uea multivariate time series classification archive, 2018, 2018.
- [3] Yanping Chen, Eamonn Keogh, Bing Hu, Nurjahan Begum, Anthony Bagnall, Abdullah Mueen, and Gustavo Batista. The UCR time series classification archive, July 2015. www.cs.ucr.edu/~eamonn/time_series_data/.
- [4] Timothée Darcet, Maxime Oquab, Julien Mairal, and Piotr Bojanowski. Vision transformers need registers, 2024.
- [5] Abhimanyu Das, Weihao Kong, Rajat Sen, and Yichen Zhou. A decoder-only foundation model for time-series forecasting. *International Conference on Machine Learning (ICML)*, 2023.
- [6] Matthijs Douze, Alexandr Guzhva, Chengqi Deng, Jeff Johnson, Gergely Szilvasy, Pierre-Emmanuel Mazaré, Maria Lomeli, Lucas Hosseini, and Hervé Jégou. The Faiss library. *arXiv*, 2024.
- [7] Vijay Ekambaram, Arindam Jati, Pankaj Dayama, Sumanta Mukherjee, Nam H Nguyen, Wesley M. Gifford, Chandra Reddy, and Jayant Kalagnanam. Tiny time mixers (TTMs): Fast pre-trained models for enhanced zero/few-shot forecasting of multivariate time series. In *The Thirty-eighth Annual Conference on Neural Information Processing Systems*, 2024.
- [8] Vijay Ekambaram, Arindam Jati, Nam Nguyen, Phanwadee Sinthong, and Jayant Kalagnanam. Tsmixer: Lightweight mlp-mixer model for multivariate time series forecasting. In *Proceedings of the 29th ACM SIGKDD Conference on Knowledge Discovery and Data Mining*, KDD ’23, page 459–469, New York, NY, USA, 2023.
- [9] Emadeldeen Eldele, Mohamed Ragab, Zhenghua Chen, Min Wu, Chee Keong Kwoh, Xiaoli Li, and Cuntai Guan. Time-series representation learning via temporal and contextual contrasting. In *Proceedings of the Thirtieth International Joint Conference on Artificial Intelligence, IJCAI-21*, pages 2352–2359, 2021.

- [10] Archibald Fraikin, Adrien Bennetot, and Stéphanie Allasonnière. T-rep: Representation learning for time series using time-embeddings, 2024.
- [11] Jean-Yves Franceschi, Aymeric Dieuleveut, and Martin Jaggi. Unsupervised scalable representation learning for multivariate time series. *Advances in neural information processing systems*, 32, 2019.
- [12] Yao Fu, Hao Peng, Litu Ou, Ashish Sabharwal, and Tushar Khot. Specializing smaller language models towards multi-step reasoning. In Andreas Krause, Emma Brunskill, Kyunghyun Cho, Barbara Engelhardt, Sivan Sabato, and Jonathan Scarlett, editors, *Proceedings of the 40th International Conference on Machine Learning*, volume 202 of *Proceedings of Machine Learning Research*, pages 10421–10430. PMLR, 23–29 Jul 2023.
- [13] Shanghua Gao, Teddy Koker, Owen Queen, Thomas Hartvigsen, Theodoros Tsiligkaridis, and Marinka Zitnik. UniTS: A unified multi-task time series model. In *The Thirty-eighth Annual Conference on Neural Information Processing Systems*, 2024.
- [14] Rakshitha Godahewa, Christoph Bergmeir, Geoffrey I. Webb, Rob J. Hyndman, and Pablo Montero-Manso. Monash time series forecasting archive. In *Neural Information Processing Systems Track on Datasets and Benchmarks*, 2021.
- [15] Mononito Goswami, Konrad Szafer, Arjun Choudhry, Yifu Cai, Shuo Li, and Artur Dubrawski. Moment: A family of open time-series foundation models. *International Conference on Machine Learning (ICML)*, 2024.
- [16] Nate Gruver, Marc Anton Finzi, Shikai Qiu, and Andrew Gordon Wilson. Large language models are zero-shot time series forecasters. In *Thirty-seventh Conference on Neural Information Processing Systems*, 2023.
- [17] Ming Jin, Shiyu Wang, Lintao Ma, Zhixuan Chu, James Y. Zhang, Xiaoming Shi, Pin-Yu Chen, Yuxuan Liang, Yuan-Fang Li, Shirui Pan, and Qingsong Wen. Time-LLM: Time series forecasting by reprogramming large language models. In *The Twelfth International Conference on Learning Representations*, 2024.
- [18] Taesung Kim, Jinhee Kim, Yunwon Tae, Cheonbok Park, Jang-Ho Choi, and Jaegul Choo. Reversible instance normalization for accurate time-series forecasting against distribution shift. In *International Conference on Learning Representations*, 2022.
- [19] Chen Ling, Xujiang Zhao, Jiaying Lu, Chengyuan Deng, Can Zheng, Junxiang Wang, Tanmoy Chowdhury, Yun Li, Hejie Cui, Xuchao Zhang, Tianjiao Zhao, Amit Panalkar, Dhagash Mehta, Stefano Pasquali, Wei Cheng, Haoyu Wang, Yanchi Liu, Zhengzhang Chen, Haifeng Chen, Chris White, Quanquan Gu, Jian Pei, Carl Yang, and Liang Zhao. Domain specialization as the key to make large language models disruptive: A comprehensive survey, 2024.
- [20] Qinghua Liu and John Paparrizos. The elephant in the room: Towards a reliable time-series anomaly detection benchmark. In A. Globerson, L. Mackey, D. Belgrave, A. Fan, U. Paquet, J. Tomczak, and C. Zhang, editors, *Advances in Neural Information Processing Systems*, volume 37, pages 108231–108261. Curran Associates, Inc., 2024.
- [21] Yong Liu, Tengge Hu, Haoran Zhang, Haixu Wu, Shiyu Wang, Lintao Ma, and Mingsheng Long. itransformer: Inverted transformers are effective for time series forecasting, 2024.
- [22] Yong Liu, Haixu Wu, Jianmin Wang, and Mingsheng Long. Non-stationary transformers: Exploring the stationarity in time series forecasting. *Advances in neural information processing systems*, 35:9881–9893, 2022.
- [23] Chien Van Nguyen, Xuan Shen, Ryan Aponte, Yu Xia, Samyadeep Basu, Zhengmian Hu, Jian Chen, Mihir Parmar, Sasidhar Kunapuli, Joe Barrow, Junda Wu, Ashish Singh, Yu Wang, Jiuxiang Gu, Franck Dernoncourt, Nesreen K. Ahmed, Nedim Lipka, Ruiyi Zhang, Xiang Chen, Tong Yu, Sungchul Kim, Hanieh Deilamsalehy, Namyong Park, Mike Rimer, Zhehao Zhang, Huanrui Yang, Ryan A. Rossi, and Thien Huu Nguyen. A survey of small language models, 2024.

- [24] Yuqi Nie, Nam H. Nguyen, Phanwadee Sinthong, and Jayant Kalagnanam. A time series is worth 64 words: Long-term forecasting with transformers. In *ICLR*, 2023.
- [25] John Paparrizos, Paul Boniol, Themis Palpanas, Ruey S Tsay, Aaron Elmore, and Michael J Franklin. Volume under the surface: a new accuracy evaluation measure for time-series anomaly detection. *Proceedings of the VLDB Endowment*, 15(11):2774–2787, 2022.
- [26] PyTorch Contributors. torch.fft.rfft — pytorch documentation <https://docs.pytorch.org/docs/stable/>, 2025. Accessed: 2025-04-23.
- [27] Kashif Rasul, Arjun Ashok, Andrew Robert Williams, Arian Khorasani, George Adamopoulos, Rishika Bhagwatkar, Marin Biloš, Hena Ghonia, Nadhir Vincent Hassen, Anderson Schneider, et al. Lag-llama: Towards foundation models for time series forecasting. *arXiv preprint arXiv:2310.08278*, 2023.
- [28] Timo Schick and Hinrich Schütze. It’s not just size that matters: Small language models are also few-shot learners. *arXiv preprint arXiv:2009.07118*, 2020.
- [29] Ilya O Tolstikhin, Neil Houlsby, Alexander Kolesnikov, Lucas Beyer, Xiaohua Zhai, Thomas Unterthiner, Jessica Yung, Andreas Steiner, Daniel Keysers, Jakob Uszkoreit, et al. Mlp-mixer: An all-mlp architecture for vision. *Advances in Neural Information Processing Systems*, 34:24261–24272, 2021.
- [30] Sana Tonekaboni, Danny Eytan, and Anna Goldenberg. Unsupervised representation learning for time series with temporal neighborhood coding. In *International Conference on Learning Representations*, 2021.
- [31] Daniel Valcarce, Alejandro Bellogín, Javier Parapar, and Pablo Castells. Assessing ranking metrics in top-N recommendation. *Information Retrieval Journal*, 23(4):411–448, June 2020.
- [32] Ashish Vaswani, Noam Shazeer, Niki Parmar, Jakob Uszkoreit, Llion Jones, Aidan N Gomez, Lukasz Kaiser, and Illia Polosukhin. Attention is all you need. In *Advances in Neural Information Processing Systems*, volume 30, 2017.
- [33] Jingyuan Wang, Jiawei Jiang, Wenjun Jiang, Chao Li, and Wayne Xin Zhao. Libcity: An open library for traffic prediction. In *Proceedings of the 29th International Conference on Advances in Geographic Information Systems*, SIGSPATIAL ’21, page 145–148, New York, NY, USA, 2021.
- [34] Shiyu Wang, Haixu Wu, Xiaoming Shi, Tengge Hu, Huakun Luo, Lintao Ma, James Y Zhang, and JUN ZHOU. Timemixer: Decomposable multiscale mixing for time series forecasting. In *International Conference on Learning Representations (ICLR)*, 2024.
- [35] Yunshi Wen, Tengfei Ma, Lily Weng, Lam Nguyen, and Anak Agung Julius. Abstracted shapes as tokens-a generalizable and interpretable model for time-series classification. *Advances in Neural Information Processing Systems*, 37:92246–92272, 2024.
- [36] Gerald Woo, Chenghao Liu, Akshat Kumar, Caiming Xiong, Silvio Savarese, and Doyen Sahoo. Unified training of universal time series forecasting transformers. *International Conference on Machine Learning (ICML)*, 2024.
- [37] Haixu Wu, Tengge Hu, Yong Liu, Hang Zhou, Jianmin Wang, and Mingsheng Long. Timesnet: Temporal 2d-variation modeling for general time series analysis. In *The Eleventh International Conference on Learning Representations*, 2022.
- [38] Haixu Wu, Jiehui Xu, Jianmin Wang, and Mingsheng Long. Autoformer: Decomposition transformers with Auto-Correlation for long-term series forecasting. In *Advances in Neural Information Processing Systems*, 2021.
- [39] Ling Yang and Shenda Hong. Unsupervised time-series representation learning with iterative bilinear temporal-spectral fusion. In *ICML*, 2022.
- [40] Zhihan Yue, Yujing Wang, Juanyong Duan, Tianmeng Yang, Congrui Huang, Yunhai Tong, and Bixiong Xu. Ts2vec: Towards universal representation of time series. In *Proceedings of the AAAI Conference on Artificial Intelligence*, volume 36, pages 8980–8987, 2022.

- [41] Ailing Zeng, Muxi Chen, Lei Zhang, and Qiang Xu. Are transformers effective for time series forecasting? *arXiv preprint arXiv:2205.13504*, 2022.
- [42] Haoyi Zhou, Shanghang Zhang, Jieqi Peng, Shuai Zhang, Jianxin Li, Hui Xiong, and Wancai Zhang. Informer: Beyond efficient transformer for long sequence time-series forecasting. In *The Thirty-Fifth AAAI Conference on Artificial Intelligence*, volume 35, pages 11106–11115, 2021.
- [43] Tian Zhou, Ziqing Ma, Qingsong Wen, Xue Wang, Liang Sun, and Rong Jin. FEDformer: Frequency enhanced decomposed transformer for long-term series forecasting. In *Proc. 39th International Conference on Machine Learning*, 2022.
- [44] Tian Zhou, Peisong Niu, Xue Wang, Liang Sun, and Rong Jin. One Fits All: Power general time series analysis by pretrained lm. In *NeurIPS*, 2023.

A Technical Appendices and Supplementary Material

A.1 Source Code and Reproducibility

The pretrained models, source code, and example scripts are included in the supplementary ZIP file for reviewer access. Full resources for reproducibility will be open-sourced publicly following the conclusion of the double-blind review process

A.2 Notation Details

In this section, we detail the notations used in the architecture for clarity. Table 2 has the notation summary.

Symbol	Description
S	Sequence length
C	Number of input channels
pl	Patch length
D	Feature dimension
$\mathbf{M} \in \mathbb{R}^{1 \times pl}$	Mask token
$\mathbf{X} \in \mathbb{R}^{S \times C}$	Multivariate time series input
$\hat{\mathbf{X}} \in \mathbb{R}^{S \times C}$	Masked time series
$\mathbf{X}_m \in \mathbb{R}^{S \times C}$	Masked and scaled input time series
$\mathbf{X}'_m \in \mathbb{R}^{C \times N \times pl}$	Transposed and patched \mathbf{X}_m
$\mathbf{X}^f \in \mathbb{R}^{S \times C}$	Normalized frequency domain ground truth signal
$\mathbf{X}^f_{\text{prob}} \in \mathbb{R}^{S/2 \times C}$	Normalized frequency probability ground truth signal
$\mathbf{X}^f_m \in \mathbb{R}^{S \times C}$	Normalized frequency domain masked signal
$\mathbf{X}'^f_m \in \mathbb{R}^{C \times N \times pl}$	Transposed and patched \mathbf{X}^f_m
$\mathbf{X}_{\text{future}} \in \mathbb{R}^{F \times C}$	Ground-truth short forecast of length F
$\mathbf{Time}_E \in \mathbb{R}^{C \times N \times D}$	Time-encoded features
$\mathbf{FFT}_E \in \mathbb{R}^{C \times N \times D}$	Frequency-encoded features
$\mathbf{Reg}_E \in \mathbb{R}^{C \times R \times D}$	Learnable register tokens
$\mathbf{Input}_E = [\mathbf{Time}_E; \mathbf{FFT}_E; \mathbf{Reg}_E] \in \mathbb{R}^{C \times (2N+R) \times D}$	Concatenated input to the backbone
$\mathbf{Backbone}_E \in \mathbb{R}^{C \times (2N+R) \times D}$	Output embedding from the backbone
$\mathbf{Decoder}_E \in \mathbb{R}^{C \times (2N+R) \times D}$	Output embeddings from the decoder
$\mathbf{Y} \in \mathbb{R}^{S \times C}$	Time domain signal reconstruction
$\mathbf{Y}_f \in \mathbb{R}^{S \times C}$	Frequency domain signal reconstruction
$\mathbf{Y}' \in \mathbb{R}^{S \times C}$	Time domain signal reconstructed from frequency embedding
$\mathbf{Y}^f_{\text{prob}} \in \mathbb{R}^{S/2 \times C}$	Predicted frequency probability
$\mathbf{Y}_{\text{future}} \in \mathbb{R}^{F \times C}$	Predicted short forecast of length F

Table 2: Notation Summary

A.3 Related Art

Neural Architectures for Time-Series Modelling Over the past few years, time-series analysis has benefited significantly from advances in neural architectures, particularly with the adaptation of models from NLP and vision to temporal data. Early breakthroughs came from transformer-based designs such as Informer [42], Autoformer [38], and FEDFormer [43], which extended attention mechanisms to model long-range dependencies and seasonal-trend decomposition in time-series. Despite their success, these models were soon challenged by simpler alternatives. DLinear [41] revealed that with basic principles like per-channel modeling and time-series decomposition, a linear model could match or surpass many transformer-based approaches. This raised important questions about the complexity-performance tradeoff in time-series modeling. A key turning point was the introduction of PatchTST [24], which demonstrated that transformers could be highly effective when embeddings are retrieved at the patch level instead of the time-point level. This patching strategy not

only preserved local semantics and improved scalability, but also re-established the superiority of transformers across multiple benchmarks.

To overcome the computational burden of transformers, new lightweight models began to emerge. TSMixer[8], built upon the MLP-Mixer[29] paradigm, replaced attention with feedforward mixing operations, achieving competitive performance with significantly reduced memory and latency. Similarly, iTransformer[21] introduced attention mechanisms over the variate (feature) dimension rather than the temporal axis, enabling better generalization across multivariate inputs. TimeMixer[34] leveraged multi-scale mixer blocks to simultaneously capture short- and long-term dynamics, while TimesNet [37] incorporated an inception-style architecture to disentangle intra- and inter-period patterns, enhancing its ability to model complex seasonal behaviors.

These developments highlight a growing diversity in time-series modeling strategies—from heavy transformers to fast feedforward mixers—each offering a different balance of accuracy, interpretability, and efficiency.

Unsupervised Time-Series Representation Learning Learning meaningful representations from unlabeled time-series is a foundational step for many downstream tasks, including classification, retrieval, and anomaly detection. Contrastive learning has emerged as a dominant strategy in this space. Temporal Neighborhood Coding (TNC)[30] introduced a local context-aware contrastive learning framework that defines neighborhoods over smoothed signals, pushing representations of nearby time segments closer while distinguishing distant ones. TS2Vec[40] extended this idea by contrasting hierarchical segments both temporally and across instances, achieving robust scale-invariant embeddings. T-Rep[10] focused on interpretability by encoding temporal attributes like trends and periodicity explicitly in the representation. BTSF[39] proposed a joint time-frequency contrastive approach, fusing insights from both domains to learn rich, discriminative embeddings. These methods typically employ compact architectures and are trained per dataset. While effective, their reliance on contrastive sampling limits scalability due to the quadratic growth in pairwise comparisons, making generalization across domains more challenging.

Time-Series Foundation Models Inspired by advances in foundation models from language and vision domains, the time-series community has begun exploring large-scale pretrained models capable of generalizing across datasets and tasks. These time-series foundation models (TSFMs) are typically trained using self-supervised objectives such as masked reconstruction or forecasting on millions of sequences.

Transformer-Based TSFMs: Several high-capacity models have been introduced with a focus on either task specialization or general-purpose transfer. In task-specialized models for forecasting, Chronos[1], TimesFM[5], and Moirai[36] represent key milestones. Chronos adopts a T5-style encoder-decoder trained on discretized sequences for forecasting, while TimesFM uses an autoregressive decoder with fixed-length patch tokens. Moirai leverages an encoder-only design with multi-scale patches and outputs probabilistic distributions, supporting multivariate forecasting with high fidelity. In task-specialised models for classification, VQSHAPE [35] offers state-of-the-art results with interpretability as they convert time-series in to sequence of meaningful and interpretable tokens. Generalist models such as Moment[15], GPT4TS[44], and UniTS [13] expand support to a wider set of tasks like classification, anomaly detection, and imputation. Moment employs masked reconstruction using a T5 encoder, while GPT4TS reuses a frozen GPT2 backbone with task-specific heads. UniTS introduces prompt and task tokens and replaces attention with DyLinear layers (dynamic operators) for efficient inference.

Non-Transformer TSFMs: In parallel, compact TSFMs have emerged to challenge the notion that larger is always better. TinyTimeMixer (TTM) [7] exemplifies this category by using TSMixer architecture trained on forecasting objectives. Despite having a minimal 1-5 M parameters, it delivers competitive zero/few-shot forecasting, showcasing the potential of compact FMs. However, TTM is primarily tailored for forecasting, and there is growing interest in extending this compact modeling paradigm to a broader range of downstream tasks—including anomaly detection, classification, and imputation—where efficiency remains an open challenge.

In summary, while contrastive and supervised representation learning methods are typically compact and effective, they are often trained separately on each dataset and lack transferability across domains. In contrast, TSFMs offer strong generalization by pretraining on large, diverse corpora—but at the cost

of significantly higher model complexity and computational demands. The ongoing challenge is to combine the generalization of foundation models with the compactness and efficiency of specialized architectures—an area where models like TSPulse seek to make impactful strides.

A.4 Baseline Methodologies

Refer to Table 3 for an overview of the methodologies used to report the baseline results. We either report the results directly from the associated papers or run their official/popular implementation to get the results.

Task	Model	Results Derivation	Reference (Code/Paper)
Anomaly Detection	All SOTA Models	Reported in [20]	TSB-AD-Leaderboard
Classification	MOMENT	Reported in [15]	MOMENT
	VQShape	Official Implementation	VQShape
	UniTS	Official Implementation	UniTS
	T-Rep	Reported in [10]	T-Rep
	TS2Vec	Reported in [40]	TS2Vec
	TNC	Reported in [40]	TS2Vec
	TS-TCC	Reported in [40]	TS2Vec
Imputation	T-Loss	Reported in [11]	T-Loss
	MOMENT	Official Implementation	MOMENT
	UniTS	Official Implementation	UniTS
	Statistical	Implementation	MOMENT
	TimesNet	Official Implementation	Time-Series-Library
	FEDformer	Implementation	Time-Series-Library
	Non-Stat. Transformer	Implementation	Time-Series-Library
Search	MOMENT	Official Implementation	MOMENT
	Chronos	Official Implementation	Chronos

Table 3: Summary of Baselines used in this work across different tasks

A.5 Pre-training Datasets

Pre-training utilizes a subset of $\sim 1\text{B}$ time points drawn from the Monash [14] and LibCity [33, 36] data collections. We leverage the same pre-training data as used in [7] for training our models. For Monash, we select a subset of datasets from the Monash Time Series Forecasting Repository [14]. For LibCity, we incorporated the data from the source locations. The complete list of datasets employed for pre-training is provided in Table 4. All datasets used are selected under permissive licenses that allow both open-source and commercial use.

A.6 Model Details

The default pre-training configuration for TSPulse is as follows: context length (S) = 512, patch length (pl) = 8, stride = pl , hidden feature size $D = 3 \times pl$, dropout = 0.2, head dropout = 0.2, number of backbone layers (L) = 8, number of decoder layers = 2, masking strategy = hybrid masking, training epochs = 20, and gated attention activation function = softmax. During pre-training, the backbone and the decoder are both operated in channel-independent approach, i.e., channel-mixing is not activated in the TSMixer modules.

Motivated by the success of lightweight, task-specialized pre-trained models in the language domain [28], [23], [12], [19]—which achieve strong performance through minimal task-specific adaptations—we extend this strategy to TSPulse via head reweighting during pretraining. We offer flexibility in pretraining: either by assigning equal weight to all heads or by specializing the pretraining through reweighting loss objectives to prioritize heads most relevant to the target task. Specifically, for task-specialized pre-training, we adjust the head usage and weighting as follows: (i) For anomaly detection, all heads are retained and assigned equal loss weights to facilitate triangulation across time, frequency, and forecast perspectives. (ii) For tasks such as imputation, classification, and retrieval, we emphasize $\text{Head}_{\text{time}}$ and $\text{Head}_{\text{prob}}$ by assigning them higher weights, while down-weighting or

Origin	Data Source	Temporal Granularity
Monash	wind 4 sec dataset + DRS	4-sec, 10-min, 15-min, 30-min, Hourly
	wind farms minutely dataset (no missing) + DRS	Min, 10-min, 15-min, 30-min, Hourly
	us births dataset	Daily
	solar 10 minutes dataset + DRS	10-min, 30-min, Hourly
	australian electricity demand dataset + DRS	30-min, Hourly, Daily
	kaggle web traffic dataset (no missing)	Daily
	nn5 daily dataset (no missing)	Daily
	solar 4 sec dataset + DRS	4-sec, 10-min, 15-min, 30-min, Hourly
	saugeenday dataset	Daily
	sunspot dataset (no missing)	Daily
	kdd cup 2018 dataset (no missing)	Hourly
	bitcoin dataset (no missing)	Daily
LibCity	london smart meters dataset (no missing) + DRS	30-min, Hourly, Daily
	australian weather dataset	Daily
	PEMS [03,04,07,08] + DRS	5-min, 10-min, 15-min, 30-min, Hourly
	PEMS BAY + DRS	5-min, 10-min, 15-min, 30-min, Hourly
	LOS LOOP + DRS	5-min, 10-min, 15-min, 30-min, Hourly

Table 4: **Pre-training Datasets for TSPulse.** We leverage the same pre-training data as used in [7] for training our models. Entries annotated with “+ **DRS**” reflect the application of Diversity Resolution Sampling strategy to derive versions at different lower temporal resolutions, as proposed in [7]. All pre-training datasets are strictly disjoint from evaluation sets. For example, `australian electricity demand dataset` and `australian weather dataset` are unrelated to the standard ECL and Weather datasets used in the evaluation tasks.

pruning the remaining heads to reduce task-irrelevant complexity. This enables TSPulse to refine task-specific representations while maintaining its lightweight design, facilitating efficient transfer learning across any dataset for the specified task.

Additionally, based on our validation analysis, we observe that for classification tasks - overall performance improves when using a longer patch size ($pl = 16$) with full patch/block masking during pre-training. This reflects an important insight: while block masking tends to hurt performance in realistic imputation settings (where masking follows irregular patterns - patch or point impute), it is beneficial for classification, where the objective is to learn strong semantic embeddings at the patch level. Block masking introduces more challenging pre-training conditions, helping the model extract more meaningful patch representations.

Thus, TSPulse adopts hybrid masking for all reconstruction-oriented tasks (imputation, anomaly detection, retrieval) and block masking specifically for classification-oriented pre-training. Pre-training one model per task does not pose any practical issues with TSPulse, as its pretraining is extremely fast and efficient. We can pre-train a model on the full $\sim 1\text{B}$ samples in just one day using $8 \times \text{A100}$ GPUs, enabling rapid training of task-specialized models with ease. We use $8\text{-}32$ A100 GPUs for rapidly pre-training these task-specialized models. For more details on the used evaluation datasets, hyperparameter optimization and train/valid/test split ratios, refer to the associated downstream task sections in the Appendix.

A.7 FFT Extraction Details

Since TSPulse performs masked reconstruction in both time and frequency domains, we first extract masked FFT features for processing by the backbone and prepare the corresponding ground-truth targets for loss computation.

The input time-series $\mathbf{X} \in \mathbb{R}^{S \times C}$ is scaled and masking is applied in the time domain, resulting in the scaled, masked version \mathbf{X}_m . Importantly, we avoid explicitly masking the frequency space. Instead, we directly feed the scaled, masked time-series \mathbf{X}_m into the Fast Fourier Transform (FFT) via the function `torch.fft.rfft` [26]. This operation transforms the time-domain signal into the frequency domain. By using the masked input, the transformation naturally propagates the masking into the frequency space, meaning that the same data is masked both in the time and frequency domains, making the reconstruction task more challenging. This step is critical for ensuring that information leakage does not occur between the two domains.

The FFT operation produces a complex-valued tensor of shape $\mathbb{R}^{(S/2)+1 \times C}$, where each element contains both a real and an imaginary component. This represents the signal in the frequency domain,

capturing both amplitude and phase information for each frequency bin. To maintain consistency in the output dimensions and to simplify further processing, we discard the last frequency bin, reducing the tensor shape to $\mathbb{R}^{S/2 \times C}$.

Next, we normalize the real and imaginary components separately for each channel by dividing them by their respective maximum absolute values. This step ensures that both components are within a comparable scale, preventing issues related to uneven amplitude distributions across channels. After normalization, the real and imaginary components are concatenated together to form the masked frequency-domain features $\mathbf{X}_m^f \in \mathbb{R}^{S \times C}$. This tensor is then ready for further processing by the backbone, ensuring that it is compatible with the expected input shape and aligns with the time-domain features.

We now compute two separate ground-truths from the frequency representation of the input. These ground-truths serve as targets for the reconstruction tasks during training.

First, we apply the same FFT transformation to the unmasked input, yielding the frequency-domain ground-truth representation $\mathbf{X}^f \in \mathbb{R}^{S \times C}$. This serves as the clean, unaltered frequency representation of the time-series, which will be used to guide the model’s reconstruction.

To create the second ground-truth, we compute the log-magnitude spectrum of the frequency representation \mathbf{X}^f , excluding the DC component (the first frequency bin, which represents the mean signal). The log-magnitude spectrum is computed as:

$$\text{log-magnitude}(\mathbf{X}^f) = \log \left(\sqrt{\text{Re}(\mathbf{X}^f)^2 + \text{Im}(\mathbf{X}^f)^2} \right)$$

where $\text{Re}(\mathbf{X}^f)$ and $\text{Im}(\mathbf{X}^f)$ represent the real and imaginary parts of the FFT output, respectively. The log transformation reduces the dynamic range of the frequency values, making the learning process more stable and preventing potential issues caused by extreme values in the frequency domain.

After computing the log-magnitude spectrum, we apply softmax across the frequency bins for each channel. This produces $\mathbf{X}_{\text{prob}}^f \in \mathbb{R}^{S/2 \times C}$, a normalized global frequency signature. The softmax operation converts the frequency magnitudes into a probability-like distribution, emphasizing the dominant spectral components. This normalized frequency signature serves as an auxiliary reconstruction target, encouraging the model to learn the most significant global patterns in the frequency domain.

The two ground-truth targets— \mathbf{X}^f (the raw frequency-domain representation) and $\mathbf{X}_{\text{prob}}^f$ (the normalized global frequency signature)—are used during training for the reconstruction task. The first target guides the model in recovering the original frequency representation, while the second target helps the model learn high-level semantic patterns that enhance its generalization to downstream tasks, such as classification or anomaly detection.

A.8 Time series Anomaly Detection

A.8.1 Basics

Model-based time-series anomaly detection (AD) leverages predictive models—such as *TSPulse*—to identify anomalous regions within a sequence. Any significant deviation between the model’s prediction ($\mathbf{Y} \in \mathbb{R}^{S \times C}$) and the actual observed sequence ($\mathbf{X} \in \mathbb{R}^{S \times C}$) is interpreted as a process deviation and quantified as an anomaly score, denoted by α . These scores reflect the degree of divergence and serve as indicators of potential anomalies, particularly when they represent out-of-distribution behavior.

The anomaly score is computed by aggregating the prediction error over a defined temporal window, referred to as the aggregation window, w , using Equation 1 as shown below.

$$\alpha_{\tau:\tau+w-1}(\mathbf{X}, \mathbf{Y}) = \frac{1}{wC} \sum_{i=\tau}^{\tau+w-1} \sum_{j=1}^C (\mathbf{X}_{i,j} - \mathbf{Y}_{i,j})^2 \quad (1)$$

Therefore, a smaller window size (w) is more effective for detecting point anomalies, whereas a larger window size is better suited for identifying range anomalies.

A.8.2 Implementation Details of Multi-Head Triangulation

TSPulse utilizes both time and frequency representations of time series, and produces multiple prediction outputs, each output either utilizes a specific data representation for data reconstruction or forecasting. While the reconstruction task relies on estimating data distribution, the forecasting task focuses on data evolution. Hence, errors in the reconstruction or forecasting tasks can potentially indicate different types of anomalies. We leverage multiple output streams from TSPulse ($\text{Head}_{\text{time}}$, Head_{fft} , and $\text{Head}_{\text{future}}$) to derive different anomaly scoring mechanisms:

1. $\text{Head}_{\text{time}}$: The first AD score is generated using the time reconstruction head of TSPulse. Following the notation of Equation 1, the score can be expressed as, $\alpha_{S-w:S-1}^{\text{time}}$. Here, $w < S$, i.e., the aggregation window size is smaller than the context length of the TSPulse, and the last w points from the TSPulse’s reconstruction are utilized to calculate the aggregated error. The resulting error is assigned as the anomaly score to the time point at the center of the aggregation window, and this process is repeated with a stride of one.
2. Head_{fft} : Similarly, this AD score utilizes the FFT reconstruction head of TSPulse, and can be expressed as $\alpha_{S-w:S-1}^{\text{fft}}$.
3. $\text{Head}_{\text{future}}$: Following the existing pre-trained forecasting models in TSB-AD leaderboard [20] like Chronos and TimesFM, we utilize the first time point in the forecast horizon coming out of the forecasting head of TSPulse to calculate the forecast error, and assign it to that particular time point as the anomaly score: $\alpha_S^{\text{future}}(\mathbf{X}, \mathbf{Y}_{\text{future}}) = \frac{1}{C} \sum_{j=1}^C \left(\mathbf{X}_{S,j} - [\mathbf{Y}_{\text{future}}]_{S,j} \right)^2$.
4. $\text{Head}_{\text{ensemble}}$: In this scoring mechanism, we temporally align the above three scores, and generate an ensemble score for every time point by computing the maximum of the three scores.

A.8.3 TSB-AD Leaderboard

Datasets The TSB-AD leaderboard [20] features a comprehensive collection of 1,070 time series drawn from 40 diverse datasets, all curated and annotated by human experts. It stands as one of the most recent and extensive benchmarks for anomaly detection (AD) in time series data.

The leaderboard is divided into two tracks:

- **TSB-AD-U**: Univariate time series anomaly detection,
- **TSB-AD-M**: Multivariate time series anomaly detection.

Each dataset contains one or more time series. To ensure fair evaluation, the data is split into distinct subsets. For detailed information on the data splits (evaluation and tuning), refer to Figure 3 in [20]. Here, we provide a brief summary:

- **Evaluation Data**: The TSB-AD-U and TSB-AD-M benchmarks contain 350 and 180 time series for evaluation, respectively. Their average anomaly ratios are 4.5% and 5%.
- **Small Training Data**: A short, anomaly-free (hence, unlabeled) historical segment from each evaluation time-series is provided for *optional* model training or fine-tuning. For TSPulse (FT), we utilize a fraction (20%) of this training data as validation data to perform early stopping.
- **Tuning Data**: A set of time-series different from the evaluation series are kept aside for tuning or hyperparameter optimization (HPO). All the models can leverage this tuning data and labels for finding optimal hyperparameters. A total of 48 and 20 time-series are kept for tuning for univariate and multivariate benchmarks, respectively.

Models and Workflows The TSB-AD leaderboard supports two primary workflows for anomaly detection:

- **Unsupervised AD**: Models are applied directly in zero-shot setting to the evaluation data to generate anomaly scores. TSPulse (ZS) falls into this category.

- **Semi-Supervised/Self-Supervised AD:** Models are trained or fine-tuned using the small, anomaly-free training segment before being evaluated. Note that no labels are available for the training. `TSPulse (FT)` falls into this category.

In both workflows, models are allowed to use the tuning data (with labels) for hyperparameter optimization.

The leaderboard currently reports results for 40 models across both the univariate and multivariate benchmarks, categorized into three broad sets: statistical (mostly unsupervised), neural networks (mostly self-supervised), and pre-trained/foundation models (both unsupervised and self-supervised).

HPO for TSPulse As mentioned briefly above, the TSB-AD leaderboard [20] provides separate *tuning datasets* for univariate (TSB-AD-U) and multivariate (TSB-AD-M) benchmarks. All the algorithms (including zero-shot and fine-tuned/trained models) leverage the tuning dataset for hyperparameter tuning. First, we employ the tuning data to find an optimal value of the aggregation window size, w , for the two reconstruction-based scoring mechanisms, α_w^{time} and α_w^{fft} . From a set of three candidate values (64, 96, 128), we find the optimal value, $w^* = 96$, following zero-shot VUS-PR scores obtained in the tuning datasets. Next, we utilize the tuning data for selecting the optimal scoring mechanism for each dataset. For each setting (univariate or multivariate), we perform a zero-shot inference of the TSPulse on the tuning data and generate the VUS-PR metrics for all four scoring mechanisms as stated above. Now, for each dataset, we choose the best scoring mechanism for that dataset (see Table 5 and Table 6). This is performed only once with the zero-shot workflow of TSPulse, and the selection is utilized in both zero-shot and fine-tuned workflows of TSPulse.

Dataset	Best TSPulse Output
Exathlon	Head_{fft}
IOPS	$\text{Head}_{\text{time}}$
LTDB	Head_{fft}
MGAB	$\text{Head}_{\text{future}}$
MITDB	$\text{Head}_{\text{ensemble}}$
MSL	$\text{Head}_{\text{time}}$
NAB	$\text{Head}_{\text{ensemble}}$
NEK	$\text{Head}_{\text{ensemble}}$
OPPORTUNITY	$\text{Head}_{\text{ensemble}}$
SED	$\text{Head}_{\text{future}}$
SMAP	$\text{Head}_{\text{time}}$
SMD	Head_{fft}
SVDB	Head_{fft}
Stock	$\text{Head}_{\text{future}}$
TAO	$\text{Head}_{\text{future}}$
TODS	$\text{Head}_{\text{time}}$
UCR	$\text{Head}_{\text{time}}$
WSD	$\text{Head}_{\text{ensemble}}$
YAHOO	$\text{Head}_{\text{future}}$

Table 5: Best TSPulse output head as detected on the Tuning dataset for univariate AD benchmark.

Dataset	Best TSPulse Output
CATSV2	$\text{Head}_{\text{future}}$
Exathlon	Head_{fft}
GHL	Head_{fft}
LTDB	$\text{Head}_{\text{time}}$
MITDB	$\text{Head}_{\text{ensemble}}$
MSL	$\text{Head}_{\text{time}}$
OPPORTUNITY	Head_{fft}
SMAP	$\text{Head}_{\text{ensemble}}$
SMD	$\text{Head}_{\text{ensemble}}$
SVDB	Head_{fft}
TAO	$\text{Head}_{\text{future}}$

Table 6: Best TSPulse output head as detected on the Tuning dataset for multivariate AD benchmark.

A.8.4 Full Results Tables

Table 7 shows the full version of Figure 4 containing all algorithms. VUS-PR scores for all methods except TSPulse are directly taken from [20]. Table 8 and Table 9 show the dataset-wise average VUS-PR scores of TSPulse along with SOTA algorithms.

A.9 Classification

We evaluate TSPulse on the UEA Multivariate Time Series Classification Archive [2], a widely used benchmark for multivariate time-series classification tasks. Table 10 summarizes the key

Method	VUS-PR
TSPulse (FT)	0.52
TSPulse (ZS)	0.48
Sub-PCA	0.42
KShapeAD	0.40
POLY	0.39
Series2Graph	0.39
MOMENT (FT)	0.39
MOMENT (ZS)	0.38
KMeansAD	0.37
USAD	0.36
Sub-KNN	0.35
MatrixProfile	0.35
SAND	0.34
CNN	0.34
LSTMAD	0.33
SR	0.32
TimesFM	0.30
IForest	0.30
OmniAnomaly	0.29
Lag-Llama	0.27
Chronos	0.27
TimesNet	0.26
AutoEncoder	0.26
TranAD	0.26
FITS	0.26
Sub-LOF	0.25
OFA	0.24
Sub-MCD	0.24
Sub-HBOS	0.23
Sub-OCSVM	0.23
Sub-IForest	0.22
Donut	0.20
LOF	0.17
AnomalyTransformer	0.12

(a) TSB-AD-U

Method	VUS-PR
TSPulse (FT)	0.39
TSPulse (ZS)	0.36
CNN	0.31
OmniAnomaly	0.31
PCA	0.31
LSTMAD	0.31
USAD	0.30
AutoEncoder	0.30
KMeansAD	0.29
CBLOF	0.27
MCD	0.27
OCSVM	0.26
Donut	0.26
RobustPCA	0.24
FITS	0.21
OFA	0.21
EIF	0.21
COPOD	0.20
IForest	0.20
HBOS	0.19
TimesNet	0.19
KNN	0.18
TranAD	0.18
LOF	0.14
AnomalyTransformer	0.12

(b) TSB-AD-M

Table 7: **Anomaly Detection Full Table.** VUS-PR metric (Higher is better) averaged across all time series across all datasets for all available algorithms in the TSB-AD leaderboard.

statistics of the datasets. TSPulse is designed with a base input context length of 512. To accommodate sequences of arbitrary lengths—both shorter and longer—we apply interpolation using `torch.nn.functional.interpolate` [26] to bring them to the base context length 512. Our framework supports up to 20× interpolation, enabling the model to process sequences as long as 10,000 time steps, which is sufficient for most real-world applications. Based on this context scaling capability, we benchmark TSPulse on 29 diverse UEA datasets. Importantly, none of the UEA datasets are included in the TSPulse pre-training corpus.

Since the UEA archive does not provide predefined validation splits, we randomly sample 10% of the training data to get a tuning validation set. We use the cross-entropy loss as the primary metric for performing Hyperparameter Optimization (HPO). The HPO is conducted based on the performance on the validation data, tuning the following parameters: TSLens projection size D' (1 or 2), mask ratio (0.3 or None), channel expansion factor (1 or 2), and head activation function (softmax or sigmoid). When mask ratio is enabled, block masking is applied during fine-tuning but disabled during evaluation to improve generalization and reduce overfitting. The default decoder configuration uses the *mix-channel* mode, which works effectively for most realistic channel counts (up to several hundred channels). In extreme cases where the number of channels is exceptionally high (e.g., DuckDuckGeese dataset with 1000+ channels), we disable mix-channel and revert to simple avg-pooling for computational efficiency, as the size of channel-mixer blocks scales proportionally with the number of channels. Additionally, given the very large channel count but extremely limited number of training samples in DuckDuckGeese, we employ a k-fold cross-validation for this instance for improved stability. In general, the batch size and number of epochs are chosen from a predefined pool set based on the scale of the training samples to prevent out-of-memory error and enable faster fine-tuning.

Method	CATSv2	Daphnet	Exathlon	IOFS	LITDB	MGAB	MITDB	MSL	NAB	NEK	OPPORTUNITY	Power	SED	SMAP	SMD	SVDB	SWaT	Stock	TAO	TODS	UCR	WSD	YAHOO
TSPulse (FT)	0.40	0.54	0.87	0.42	0.52	0.01	0.22	0.66	0.51	0.58	0.06	0.08	0.07	0.74	0.80	0.56	0.10	0.98	1.00	0.68	0.28	0.43	0.83
TSPulse (ZS)	0.35	0.55	0.83	0.42	0.41	0.00	0.10	0.64	0.50	0.58	0.06	0.07	0.06	0.71	0.78	0.36	0.10	0.98	1.00	0.68	0.18	0.42	0.83
Sub-PCA	0.26	0.42	0.93	0.23	0.56	0.01	0.36	0.51	0.44	0.91	0.91	0.08	0.03	0.52	0.45	0.52	0.39	0.84	0.93	0.54	0.12	0.09	0.14
KShapeAD	0.25	0.04	0.33	0.09	0.83	0.02	0.69	0.55	0.37	0.24	0.33	0.19	0.89	0.58	0.13	0.82	0.43	0.75	0.91	0.75	0.38	0.10	0.55
POLY	0.23	0.51	0.74	0.31	0.51	0.01	0.34	0.54	0.48	0.61	0.10	0.09	0.04	0.64	0.61	0.44	0.10	0.82	0.92	0.57	0.13	0.41	0.25
Series2Graph	0.21	0.19	0.60	0.22	0.79	0.00	0.61	0.25	0.44	0.67	0.11	0.07	0.15	0.55	0.46	0.55	0.22	0.79	0.91	0.73	0.25	0.27	0.28
MOMENT (FT)	0.38	0.51	0.83	0.38	0.45	0.00	0.13	0.53	0.39	0.73	0.07	0.07	0.04	0.63	0.75	0.23	0.08	0.81	0.94	0.58	0.08	0.50	0.25
MOMENT (ZS)	0.30	0.52	0.81	0.37	0.44	0.00	0.14	0.53	0.39	0.73	0.07	0.08	0.04	0.62	0.74	0.27	0.07	0.81	0.94	0.58	0.07	0.49	0.23
KMeansAD	0.23	0.04	0.41	0.06	0.49	0.01	0.27	0.48	0.33	0.20	0.30	0.39	0.87	0.63	0.18	0.44	0.10	0.76	0.92	0.65	0.38	0.10	0.56
USAD	0.40	0.12	0.89	0.13	0.55	0.00	0.18	0.27	0.28	0.73	0.67	0.06	0.03	0.27	0.66	0.43	0.37	0.75	0.93	0.52	0.08	0.04	0.10
Sub-KNN	0.29	0.04	0.47	0.10	0.58	0.24	0.36	0.33	0.29	0.23	0.30	0.21	0.87	0.51	0.14	0.56	0.10	0.75	0.92	0.65	0.37	0.10	0.31
MatrixProfile	0.36	0.04	0.56	0.10	0.58	0.29	0.39	0.48	0.32	0.13	0.25	0.15	0.72	0.47	0.13	0.36	0.11	0.72	0.92	0.76	0.34	0.02	0.43
SAND	0.27	0.04	0.25	0.06	0.79	0.01	0.67	0.30	0.38	0.32	0.18	0.16	0.75	0.56	0.11	0.72	0.21	0.74	0.91	0.70	0.34	0.08	0.41
CNN	0.32	0.40	0.61	0.26	0.42	0.01	0.15	0.33	0.19	0.73	0.40	0.08	0.06	0.34	0.55	0.21	0.68	0.92	1.00	0.54	0.05	0.24	0.53
LSTMAD	0.33	0.13	0.73	0.20	0.36	0.03	0.12	0.32	0.18	0.73	0.58	0.07	0.06	0.26	0.49	0.13	0.67	0.85	1.00	0.47	0.02	0.13	0.45
SR	0.28	0.20	0.73	0.24	0.29	0.01	0.07	0.22	0.20	0.50	0.33	0.10	0.07	0.29	0.36	0.08	0.35	1.00	1.00	0.64	0.07	0.22	0.61
TimesFM	0.25	0.36	0.53	0.20	0.27	0.00	0.06	0.32	0.18	0.35	0.05	0.08	0.05	0.30	0.40	0.06	0.22	0.99	0.99	0.75	0.07	0.21	0.81
IForest	0.08	0.36	0.67	0.28	0.34	0.00	0.10	0.29	0.22	0.59	0.43	0.08	0.36	0.25	0.34	0.09	0.50	0.99	0.99	0.52	0.02	0.14	0.44
OmniAnomaly	0.12	0.16	0.83	0.20	0.32	0.00	0.10	0.25	0.19	0.85	0.60	0.07	0.06	0.15	0.36	0.09	0.44	0.82	0.98	0.44	0.03	0.14	0.19
Lag-Llama	0.21	0.39	0.53	0.22	0.29	0.00	0.08	0.31	0.18	0.38	0.05	0.08	0.07	0.28	0.36	0.08	0.09	0.97	0.99	0.61	0.02	0.22	0.68
Chronos	0.10	0.31	0.45	0.18	0.26	0.00	0.06	0.18	0.18	0.34	0.06	0.08	0.06	0.19	0.32	0.06	0.14	0.99	1.00	0.70	0.07	0.18	0.80
TimesNet	0.10	0.39	0.53	0.22	0.29	0.00	0.08	0.31	0.20	0.37	0.05	0.08	0.05	0.38	0.54	0.09	0.11	0.79	0.91	0.59	0.02	0.27	0.29
AutoEncoder	0.18	0.09	0.36	0.25	0.69	0.01	0.07	0.27	0.32	0.51	0.12	0.09	0.41	0.49	0.14	0.32	0.38	0.72	0.93	0.65	0.09	0.14	0.29
TranAD	0.08	0.13	0.72	0.18	0.31	0.00	0.09	0.18	0.18	0.72	0.58	0.07	0.05	0.13	0.16	0.09	0.46	0.79	0.94	0.45	0.02	0.11	0.28
FITS	0.17	0.43	0.55	0.17	0.34	0.00	0.09	0.36	0.24	0.49	0.07	0.07	0.05	0.42	0.54	0.10	0.10	0.76	0.91	0.58	0.02	0.14	0.18
Sub-LOF	0.31	0.04	0.25	0.11	0.34	0.44	0.26	0.35	0.32	0.25	0.12	0.14	0.22	0.40	0.04	0.18	0.11	0.76	0.92	0.53	0.29	0.03	0.27
OFA	0.16	0.36	0.55	0.20	0.30	0.00	0.07	0.29	0.21	0.37	0.05	0.08	0.06	0.33	0.45	0.07	0.11	0.76	0.91	0.54	0.02	0.16	0.24
Sub-MCD	0.37	0.04	0.23	0.13	0.24	0.01	0.11	0.16	0.19	0.11	0.32	0.30	0.12	0.30	0.08	0.07	0.09	0.75	0.90	0.64	0.26	0.15	0.28
Sub-HBOS	0.04	0.05	0.45	0.05	0.69	0.00	0.17	0.25	0.30	0.23	0.08	0.12	0.88	0.55	0.10	0.24	0.12	0.70	0.93	0.64	0.14	0.01	0.06
Sub-OCSVM	0.26	0.06	0.29	0.07	0.33	0.01	0.14	0.28	0.26	0.26	0.11	0.16	0.06	0.51	0.08	0.20	0.09	0.73	0.92	0.65	0.18	0.03	0.23
Sub-IForest	0.05	0.07	0.49	0.04	0.66	0.00	0.24	0.36	0.30	0.22	0.07	0.12	0.79	0.47	0.09	0.27	0.13	0.69	0.90	0.66	0.10	0.01	0.06
Donut	0.08	0.06	0.45	0.10	0.31	0.00	0.10	0.20	0.18	0.47	0.18	0.09	0.14	0.31	0.29	0.08	0.47	0.78	0.91	0.48	0.01	0.06	0.12
LOF	0.06	0.13	0.20	0.12	0.26	0.00	0.06	0.15	0.17	0.38	0.14	0.09	0.11	0.15	0.13	0.05	0.12	0.75	0.91	0.49	0.02	0.09	0.37
AnomalyTransformer	0.05	0.07	0.13	0.06	0.27	0.00	0.09	0.14	0.14	0.23	0.07	0.09	0.09	0.09	0.18	0.07	0.10	0.75	0.90	0.46	0.01	0.02	0.07

Table 8: **VUS-PR score (Higher is better) averaged over all time series for each dataset** for univariate anomaly detection. Note that every dataset has one or more time series, and the mean scores reported in Figure 4a in the main text and Table 7 above are averaged over all 350 “Eval” time series (similar to the TSB-AD-U leaderboard). This table can be compared with the dataset-wise Table-6 of [20].

Method	CATSv2	CreditCard	Daphnet	Exathlon	GECCO	GHL	Genesis	LITDB	MITDB	MSL	OPPORTUNITY	PSM	SMAP	SMD	SVDB	SWaT	TAO
TSPulse (FT)	0.07	0.00	0.35	0.91	0.18	0.01	0.02	0.57	0.14	0.21	0.07	0.14	0.32	0.36	0.47	0.14	0.93
TSPulse (ZS)	0.05	0.00	0.35	0.89	0.17	0.01	0.01	0.36	0.07	0.20	0.07	0.14	0.30	0.35	0.38	0.13	0.93
CNN	0.08	0.02	0.21	0.68	0.03	0.02	0.10	0.33	0.14	0.35	0.16	0.22	0.19	0.35	0.19	0.41	1.00
OmniAnomaly	0.04	0.02	0.34	0.84	0.02	0.07	0.00	0.44	0.11	0.22	0.18	0.16	0.12	0.17	0.35	0.15	0.81
PCA	0.12	0.10	0.13	0.95	0.20	0.01	0.02	0.24	0.07	0.15	0.30	0.16	0.09	0.36	0.11	0.45	1.00
LSTMAD	0.04	0.02	0.31	0.82	0.02	0.06	0.04	0.30	0.09	0.22	0.17	0.24	0.16	0.33	0.15	0.16	0.99
USAD	0.04	0.02	0.34	0.84	0.02	0.06	0.00	0.41	0.12	0.23	0.18	0.19	0.11	0.16	0.32	0.15	0.81
AutoEncoder	0.06	0.03	0.13	0.91	0.05	0.05	0.01	0.21	0.04	0.22	0.14	0.28	0.13	0.30	0.06	0.58	1.00
KMeansAD	0.12	0.02	0.30	0.37	0.06	0.03	0.89	0.41	0.06	0.44	0.06	0.21	0.38	0.36	0.20	0.16	0.86
CBLOF	0.06	0.03	0.10	0.86	0.03	0.02	0.02	0.20	0.04	0.21	0.14	0.19	0.14	0.22	0.07	0.29	1.00
MCD	0.13	0.06	0.14	0.80	0.03	0.01	0.06	0.21	0.04	0.23	0.17	0.26	0.10	0.26	0.07	0.54	1.00
OCSVM	0.08	0.02	0.06	0.83	0.04	0.04	0.08	0.20	0.04	0.22	0.12	0.19	0.12	0.28	0.06	0.44	0.81
Donut	0.07	0.02	0.17	0.66	0.03	0.05	0.18	0.26	0.12	0.30	0.15	0.20	0.18	0.19	0.11	0.44	0.75
RobustPCA	0.04	0.02	0.06	0.77	0.02	0.03	0.00	0.23	0.04	0.22	0.13	0.12	0.07	0.10	0.08	0.12	1.00
FITS	0.13	0.02	0.33	0.63	0.03	0.01	0.10	0.23	0.05	0.17	0.05	0.13	0.08	0.17	0.10	0.15	0.78
OFA	0.13	0.02	0.31	0.58	0.04	0.01	0.22	0.29	0.06	0.14	0.05	0.17	0.08	0.17	0.12	0.12	0.78
EIF	0.06	0.02	0.15	0.41	0.04	0.02	0.06	0.19	0.04	0.18	0.10	0.18	0.13	0.32	0.07	0.32	0.89
COPOD	0.05	0.05	0.11	0.40	0.04	0.03	0.08	0.21	0.04	0.21	0.17	0.20	0.10	0.19	0.07	0.31	0.99
IForest	0.05	0.03	0.13	0.35	0.04	0.05	0.08	0.21	0.04	0.21	0.18	0.19	0.09	0.26	0.07	0.39	0.93
HBOS	0.05	0.04	0.15	0.32	0.04	0.04	0.08	0.21	0.04	0.23	0.17	0.17	0.09	0.25	0.07	0.30	0.83
TimesNet	0.07	0.02	0.27	0.42	0.03	0.01	0.02	0.27	0.07	0.17	0.06	0.14	0.09	0.14	0.11	0.14	0.79
KNN	0.07	0.02	0.25	0.33	0.11	0.01	0.04	0.19	0.04	0.18	0.06	0.12	0.12	0.30	0.06	0.11	0.78
TranAD	0.04	0.02	0.31	0.10	0.02	0.06	0.04	0.26	0.07	0.24	0.16	0.23	0.09	0.30	0.12	0.15	0.81
LOF	0.05	0.02	0.11	0.16	0.13	0.01	0.08	0.19	0.04	0.14	0.10	0.15	0.09	0.16	0.06	0.15	0.79
AnomalyTransformer	0.03	0.02	0.07	0.10	0.02	0.03	0.01	0.21	0.05	0.12	0.07	0.21	0.06	0.07	0.08	0.18	0.77

Table 9: **VUS-PR score (Higher is better) averaged over all time series for each dataset** for multivariate anomaly detection. Note that every dataset has one or more time series, and the mean scores reported in Figure 4b in the main text and Table 7 above are averaged over all 180 “Eval” time series (similar to the TSB-AD-M leaderboard). This table can be compared with the dataset-wise Table-7 of [20].

We benchmark TSPulse on classification against a broad set of baselines, including recent pre-trained models (MOMENT [15], VQShape [35], UniTS [13]) and data-specific methods (T-Rep [10], TS2Vec [40], TNC [30], T-Loss [11], TS-TCC [9]). As detailed in the Table 3, we either report the results directly from the paper or run their official implementation. Specifically, for UniTS, we adopt the prompt-tuned (PMT) approach proposed in their paper [13], applying it to the available pretrained model across all 29 datasets in a multi-task setting and report the resulting accuracy. The overall classification results, including comparisons against baselines, are presented in Table 11, and detailed ablation studies are shown in Table 12.

ID	Dataset	# of {Train, Test} Samples	Classes	{Length, Channels}
1	ArticularyWordRecognition	{275, 300}	25	{144, 9}
2	AtrialFibrillation	{15, 15}	3	{640, 2}
3	BasicMotions	{40, 40}	4	{100, 6}
4	Cricket	{108, 72}	12	{1197, 6}
5	Epilepsy	{137, 138}	4	{206, 3}
6	EthanolConcentration	{261, 263}	4	{1751, 3}
7	ERing	{30, 30}	6	{65, 4}
8	FingerMovements	{316, 100}	2	{50, 28}
9	HandMovementDirection	{320, 147}	4	{400, 10}
10	Handwriting	{150, 850}	26	{152, 3}
11	JapaneseVowels	{270, 370}	9	{29, 12}
12	Libras	{180, 180}	15	{45, 2}
13	LSST	{2459, 2466}	14	{36, 6}
14	MotorImagery	{278, 100}	2	{3000, 64}
15	NATOPS	{180, 180}	6	{51, 24}
16	RacketSports	{151, 152}	4	{30, 6}
17	SelfRegulationSCP1	{268, 293}	2	{896, 6}
18	SelfRegulationSCP2	{200, 180}	2	{1152, 7}
19	SpokenArabicDigits	{6599, 2199}	10	{93, 13}
20	StandWalkJump	{12, 15}	3	{2500, 4}
21	UWaveGestureLibrary	{120, 320}	8	{315, 3}
22	PEMS-SF	{267, 173}	7	{144, 963}
23	Phoneme	{3315, 3353}	39	{217, 11}
24	PenDigits	{7494, 3498}	10	{8, 2}
25	Heartbeat	{204, 205}	2	{405, 61}
26	FaceDetection	{5890, 3524}	2	{62, 144}
27	CharacterTrajectories	{1422, 1436}	20	{182, 3}
28	DuckDuckGeese	{60, 40}	5	{270, 1345}
29	InsectWingbeat	{30000, 20000}	10	{78, 200}

Table 10: Summary of the UEA Multivariate Time Series Classification Archive (2018)[2]

Dataset	TSPulse	VQShape	MOMENT	UniTS	T-Rep	TS2Vec	T-Loss	TNC	TS-TCC
ArticulatoryWordRecognition	0.98	0.987	0.99	0.947	0.968	0.987	0.943	0.973	0.953
AtrialFibrillation	0.467	0.52	0.2	0.2	0.354	0.2	0.133	0.133	0.267
BasicMotions	1.0	0.885	1.0	0.8	1.0	0.975	1.0	0.975	1.0
CharacterTrajectories	0.987	0.962	0.964*	0.968	0.989	0.995	0.993	0.967	0.985
Cricket	0.917	0.975	0.986	0.958	0.958	0.972	0.972	0.958	0.917
DuckDuckGeese	0.72	0.344	0.6	0.26	0.457	0.68	0.65	0.46	0.38
ERing	0.937	0.947	0.959	0.841	0.943	0.874	0.133	0.852	0.904
Epilepsy	0.971	0.755	0.993	0.949	0.97	0.964	0.971	0.957	0.957
EthanolConcentration	0.247	0.306	0.357	0.266	0.333	0.308	0.205	0.297	0.285
FaceDetection	0.675	0.653	0.633	0.569	0.581	0.501	0.513	0.536	0.544
FingerMovements	0.53	0.616	0.49	0.53	0.495	0.48	0.58	0.47	0.46
HandMovementDirection	0.649	0.514	0.324	0.284	0.536	0.338	0.351	0.324	0.243
Handwriting	0.215	0.266	0.308	0.149	0.414	0.515	0.451	0.249	0.498
Heartbeat	0.702	0.632	0.722	0.61	0.725	0.683	0.741	0.746	0.75
InsectWingbeat	0.723	NA	0.246	0.484	0.328	0.466	0.156	0.469	0.264
JapaneseVowels	0.976	0.941	0.716	0.851	0.962	0.984	0.989	0.978	0.93
LSST	0.518	0.511	0.411	0.467	0.526	0.537	0.509	0.595	0.474
Libras	0.767	0.808	0.85	0.756	0.829	0.867	0.883	0.817	0.822
MotorImagery	0.58	0.638	0.5	0.49	0.495	0.51	0.58	0.5	0.61
NATOPS	0.878	0.804	0.828	0.75	0.804	0.928	0.917	0.911	0.822
PEMS-SF	0.855	0.85	0.896	0.855	0.8	0.682	0.676	0.699	0.734
PenDigits	0.969	0.973	0.972	0.956	0.971	0.989	0.981	0.979	0.974
PhonemeSpectra	0.156	0.087	0.233	0.173	0.232	0.233	0.222	0.207	0.252
RacketSports	0.901	0.838	0.796	0.697	0.883	0.855	0.855	0.776	0.816
SelfRegulationSCP1	0.836	0.889	0.84	0.823	0.819	0.812	0.843	0.799	0.823
SelfRegulationSCP2	0.511	0.586	0.478	0.556	0.591	0.578	0.539	0.55	0.533
SpokenArabicDigits	0.984	0.976	0.981	0.957	0.994	0.988	0.905	0.934	0.97
StandWalkJump	0.733	0.707	0.4	0.4	0.441	0.467	0.333	0.4	0.333
UWaveGestureLibrary	0.881	0.879	0.909	0.85	0.885	0.906	0.875	0.759	0.753
Mean	0.733	0.701	0.675	0.634	0.699	0.699	0.652	0.665	0.664
IMP(%)		5%	9%	16%	5%	5%	12%	10%	10%

Table 11: **Classification accuracy results (Higher is better) on UEA datasets.** We report both the mean accuracy and the IMP (%)—the percentage improvement of TSPulse over each baseline in terms of mean accuracy. On the InsectWingbeat dataset, VQShape encountered an out-of-memory (OOM) error due to the large data volume and its relatively large model size. Accordingly, the VQShape result is reported as NA for this dataset. However, for averaging purposes, we substitute the best-performing baseline result in place of VQShape to maintain consistency in the overall mean accuracy comparison. *For CharacterTrajectories dataset we used the official implementation of MOMENT to get the results.

A.10 Imputation

Dataset We evaluate TSPulse and several baseline methods on six real-world datasets from the LTSF benchmark suite [38]—ETTh1, ETTh2, ETTm1, ETTm2, Weather, and Electricity. We use context length = 512, stride = 1 and the same train/valid/test split ratio as proposed in [38].

Masking Strategies We assess model performance under two masking regimes: *block masking* and *hybrid masking*, defined as follows:

- **Block Masking:** This setup simulates scenarios like sensor failures or maintenance intervals, where data is missing in contiguous segments. Specifically, blocks of 8 consecutive time-points (i.e. full patch) are masked and must be reconstructed by the model.
- **Hybrid Masking:** To reflect more realistic settings, this scheme introduces both structured and unstructured missingness. Half of the missing points occur in full-length patches (8-point blocks), while the other half are scattered randomly across the sequence. This design captures a mix of localized and irregular masking patterns.

Baselines To evaluate the effectiveness of TSPulse under both masking setups, we benchmark it against a diverse set of baselines categorized as follows:

- **Zero-Shot / Prompt-Tuned / Statistical:** We include two recent pre-trained models—MOMENT (large)[15] and UniTS[13]. MOMENT is evaluated in a pure zero-shot manner, consistent with TSPulse. UniTS is prompt-tuned using 10% of the dataset (across all six benchmarks) in a multi-task setting, as per the original implementation.

Data	TSPulse	w/o Short Emb	w/o Long Emb	w/o Mask	w/o CM Identity Init	w/o Channel Expansion	w/o TSLens (Avg-Pool)	w/o TSLens (Max-Pool)	w/o Dual-space
ArticulatoryWordRecognition	0.98	0.973	0.963	0.983	0.973	0.987	0.973	0.953	0.98
AtrialFibrillation	0.467	0.267	0.333	0.333	0.333	0.467	0.333	0.333	0.467
BasicMotions	1.0	1.0	0.975	1.0	0.975	0.975	0.975	0.875	1.0
Cricket	0.917	0.944	0.917	0.944	0.944	0.931	0.972	0.986	0.944
ERing	0.937	0.922	0.889	0.919	0.922	0.937	0.837	0.848	0.915
Epilepsy	0.971	0.986	0.942	0.978	0.964	0.971	0.957	0.899	0.949
EthanolConcentration	0.247	0.262	0.247	0.262	0.251	0.259	0.319	0.243	0.266
FingerMovements	0.53	0.52	0.54	0.51	0.57	0.52	0.46	0.44	0.48
HandMovementDirection	0.649	0.486	0.486	0.351	0.527	0.649	0.473	0.351	0.473
Handwriting	0.215	0.189	0.055	0.215	0.199	0.026	0.034	0.182	0.175
JapaneseVowels	0.976	0.976	0.97	0.968	0.959	0.981	0.968	0.719	0.97
MotorImagery	0.58	0.47	0.52	0.58	0.52	0.58	0.47	0.47	0.49
NATOPS	0.878	0.817	0.861	0.861	0.811	0.878	0.894	0.778	0.872
RacketSports	0.901	0.816	0.803	0.783	0.829	0.842	0.842	0.809	0.803
SelfRegulationSCP1	0.836	0.802	0.829	0.836	0.853	0.836	0.867	0.816	0.853
StandWalkJump	0.733	0.4	0.4	0.333	0.133	0.733	0.267	0.4	0.333
UWaveGestureLibrary	0.881	0.878	0.847	0.891	0.875	0.9	0.825	0.859	0.866
Mean	0.747	0.689	0.681	0.691	0.685	0.734	0.675	0.645	0.696
IMP(%)		8%	10%	8%	9%	2%	11%	16%	7%

Table 12: **Classification Ablation study (Higher is better)**. We report both the mean accuracy and the IMP (%)—the percentage improvement of TSPulse over each dropped component in terms of the mean accuracy.

MOMENT Setup: For block masking, missing patches are replaced with the learned mask token in the embedding space, following [15]. In hybrid masking, we adopt a mixed approach—using the mask token for fully missing 8-point patches and zeros for the irregularly missing points. This **Heterogeneous** strategy consistently outperformed the simpler **Only-zeros** strategy (where all missing points are zeroed out) for MOMENT, as detailed in Table 19.

UniTS Setup: We similarly compare **Heterogeneous** and **Only-zeros** masking strategies. For UniTS, the **Only-zeros** approach yielded better results—likely due to prompt tuning on 10% of the data, allowing the model to better adapt to uniformly zero-masked inputs than to a mix of learned tokens and zeros. Full ablations are shown in Table 19.

Note: TSPulse uses a single learnable raw-level mask patch, enabling it to uniformly handle both block and hybrid masking without requiring masking strategy-specific adjustments.

In addition to these pre-trained models, we evaluate four classical interpolation methods: Naive, Linear, Nearest, and Cubic.

- **Fine-Tuned / Supervised:** We include fully supervised baselines—TimesNet [37], Non-Stationary Transformer (Non-Stat.) [22], and FEDformer [43]—trained end-to-end on the complete datasets individually. These are compared against the fine-tuned variant of TSPulse (TSPulse-FT).

Results Figure 6 and Figure 8 summarizes TSPulse’s imputation performance across all six datasets and masking ratios under hybrid and block masking setups respectively. Detailed per-dataset results averaged over four mask ratios are presented in Table 13. Complete breakdowns for each dataset and ratio are provided in Table 14 (hybrid masking) and Table 15 (block masking).

Ablation study As shown in Table 17, removing dual-space reconstruction during pre-training results in a consistent 8% drop in zero-shot imputation accuracy for hybrid mask set-up. Furthermore, when pre-training is done with only block masking (i.e w/o Hybrid pre-training), model suffers a drastic 79% drop hybrid-masked settings, where missingness is irregular and more reflective of real-world scenarios. This sharp contrast underscores the critical role of hybrid-masking during pre-training for achieving robust, generalizable imputation across diverse masking patterns.

A.11 Similarity Search

We evaluate the zero-shot similarity search capabilities of **TSPulse**, using its short register embeddings (i.e. zero-shot semantic embeddings) to identify time-series segments that share similar patterns with a given query, even under real-world distortions such as time shifts, magnitude changes, and additive noise. Such similarity search is valuable in practical time-series analysis, where retrieving similar

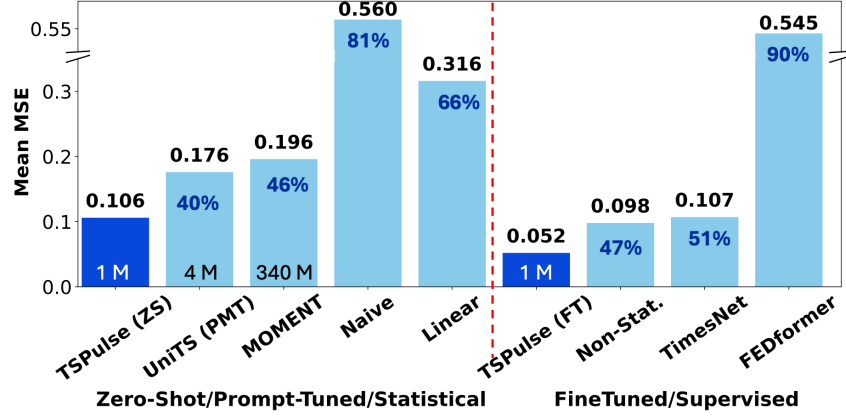


Figure 8: **Block Masking imputation MSE results (lower is better)**. Averaged across 6 LTSF benchmark datasets [38]: ETTh1, ETTh2, ETTm1, ETTm2, Weather, and Electricity, under 4 mask ratios (12.5%, 25%, 37.5%, 50%)

Dataset	Block_Masking									Hybrid_Masking								
	ZS/PMT/Statistical					FT/SUP				ZS/PMT/Statistical					FT/SUP			
	TSP_ZS	UTS_PMT	MNT	Naive	Lin.	TSP_FT	Non-Stat.	TNT	FED	TSP_ZS	UTS_PMT	MNT	Naive	Lin.	TSP_FT	Non-Stat.	TNT	FED
ETTh1	0.238	<u>0.284</u>	0.401	1.106	0.677	0.088	<u>0.174</u>	0.190	0.416	0.163	<u>0.269</u>	0.437	0.675	0.346	0.060	<u>0.123</u>	0.129	0.269
ETTh2	0.095	0.239	<u>0.134</u>	0.228	0.140	0.058	0.115	<u>0.114</u>	1.124	0.070	0.254	0.302	0.155	<u>0.093</u>	0.046	0.093	<u>0.085</u>	0.629
ETTh1	0.094	0.195	0.224	0.437	<u>0.157</u>	0.035	<u>0.076</u>	0.098	0.335	0.057	0.172	0.270	0.197	<u>0.070</u>	0.024	0.053	0.059	0.195
ETTh2	0.054	0.132	0.082	0.113	<u>0.062</u>	0.030	<u>0.052</u>	0.060	0.895	0.037	0.122	0.247	0.070	<u>0.039</u>	0.023	0.041	<u>0.040</u>	0.422
Weather	0.056	0.078	0.081	0.107	<u>0.062</u>	0.040	0.060	<u>0.056</u>	0.229	0.039	0.072	0.107	0.071	<u>0.042</u>	0.034	0.045	<u>0.044</u>	0.132
Electricity	0.097	0.126	0.252	1.371	0.797	0.060	0.114	0.126	0.271	0.077	0.130	0.293	0.808	0.378	0.049	0.104	0.122	0.236
Mean	0.106	0.176	0.196	0.560	0.316	0.052	0.098	0.107	0.545	0.074	0.170	0.276	0.329	0.161	0.039	0.076	0.08	0.314
% IMP. of TSP_ZS	—	40%	46%	81%	66%	—	—	—	—	—	56%	73%	78%	54%	—	—	—	—
% IMP. of TSP_FT	—	—	—	—	—	—	47%	51%	90%	—	—	—	—	—	—	49%	51%	88%

Table 13: **Imputation Result (MSE, Lower is better): Hybrid and Block masking setup averaged across all 4 mask ratios.** Lowest MSE score across models is highlighted in **Bold** and second lowest MSE score is underlined.

Abbreviations: FT : Finetuned, PMT : Prompt_Tuned, SUP : Supervised, ZS : Zeroshot, TSP : TSPulse, MNT : MOMENT, UTS : UniTS, TNT : TimesNet, Lin. : Linear Interpolation, Non-Stat. : Non-Stationary Transformer, FED : FEDformer. Refer to Table 14 and Table 15 for detailed results

patterns from historical data is often essential for interpretability and post-diagnostics—for example, understanding the context of a detected anomaly or performing root-cause analysis by matching query patterns to historical logs.

This task is particularly challenging because time-series data are typically long and stored as short windows using high-stride sliding windows to reduce indexing memory. This leads to the same underlying pattern appearing at different positions across windows - making exact alignment between query and index samples unlikely. Thus, models must learn robust and distortion-invariant embeddings to enable effective retrieval.

Datasets We construct two benchmark datasets—one synthetic and one real-world, which are indexed for retrieval:

- **Synthetic Dataset:** We begin with 8 distinct base patterns (see Table 20) and form 56 unique combinations by pairing them through addition and multiplication operations ($8C_2 \times 2$). Each combination is then varied by a frequency parameter $f = 1, \dots, 10$. Light augmentations—1% Gaussian noise and 1% magnitude scaling—are applied to each sample, resulting in three variants per time-series. This process yields a total of $56 \times 10 \times 3 = 1,680$ indexed time-series segments.
- **Real Dataset:** We use the UCR Archive [3], which consists of 128 time-series classification datasets. For each class in each dataset, we randomly sample 10 time-series segments of

Dataset	MR	Zeroshot/Prompt_Tuned/Statistical							Finetuned/Supervised			
		TSPulse	UniTS (PMT)	MOMENT	Naive	Linear	Nearest	Cubic	TSPulse	Non-Stationary Transformer	TimesNet	FED-former
ETTh1	0.125	0.146	0.220	0.324	0.608	0.284	0.388	0.491	0.042	<u>0.089</u>	0.098	0.180
	0.250	0.155	0.250	0.387	0.648	0.321	0.425	0.618	0.051	<u>0.113</u>	0.120	0.241
	0.375	0.168	0.287	0.468	0.696	0.365	0.471	0.791	0.065	0.135	<u>0.127</u>	0.298
	0.500	0.183	0.319	0.568	0.749	0.414	0.525	1.011	0.081	<u>0.156</u>	0.169	0.358
	Mean	0.163	<u>0.269</u>	0.437	0.675	0.346	0.452	0.728	0.060	<u>0.123</u>	0.129	0.269
ETTh2	0.125	0.065	0.151	0.132	0.143	0.084	0.114	0.296	0.041	0.081	<u>0.071</u>	0.375
	0.250	0.068	0.199	0.202	0.150	<u>0.090</u>	0.119	0.358	0.043	0.088	<u>0.080</u>	0.553
	0.375	0.072	0.300	0.332	0.159	<u>0.095</u>	0.124	0.430	0.047	0.097	<u>0.088</u>	0.716
	0.500	0.077	0.364	0.542	0.169	<u>0.103</u>	0.132	0.505	0.053	0.104	<u>0.100</u>	0.873
	Mean	0.070	0.254	0.302	0.155	<u>0.093</u>	0.122	0.397	0.046	0.093	<u>0.085</u>	0.629
ETTm1	0.125	0.049	0.123	0.156	0.154	<u>0.056</u>	0.091	0.173	0.018	<u>0.040</u>	0.048	0.109
	0.250	0.053	0.156	0.218	0.179	<u>0.064</u>	0.101	0.210	0.022	<u>0.048</u>	0.058	0.169
	0.375	0.058	0.187	0.299	0.209	<u>0.073</u>	0.114	0.254	0.026	<u>0.057</u>	0.061	0.225
	0.500	0.066	0.222	0.407	0.248	<u>0.086</u>	0.131	0.305	0.031	<u>0.067</u>	0.070	0.275
	Mean	0.057	0.172	0.270	0.197	<u>0.070</u>	0.109	0.235	0.024	<u>0.053</u>	0.059	0.195
ETTm2	0.125	0.034	0.096	0.085	0.063	<u>0.036</u>	0.049	0.115	0.020	<u>0.035</u>	0.036	0.214
	0.250	0.036	0.092	0.149	0.067	<u>0.038</u>	0.052	0.139	0.022	0.039	<u>0.038</u>	0.353
	0.375	0.038	0.126	0.272	0.072	<u>0.040</u>	0.055	0.171	0.024	0.042	<u>0.041</u>	0.492
	0.500	0.041	0.172	0.480	0.079	<u>0.044</u>	0.058	0.207	0.026	0.047	<u>0.045</u>	0.628
	Mean	0.037	0.122	0.247	0.070	<u>0.039</u>	0.054	0.158	0.023	0.041	<u>0.040</u>	0.422
Weather	0.125	0.036	0.059	0.069	0.065	<u>0.038</u>	0.053	0.131	0.036	0.040	<u>0.039</u>	0.076
	0.250	0.038	0.070	0.086	0.068	<u>0.040</u>	0.055	0.163	0.033	0.043	<u>0.042</u>	0.106
	0.375	0.040	0.074	0.115	0.072	<u>0.043</u>	0.057	0.190	0.033	<u>0.045</u>	0.046	0.148
	0.500	0.042	0.085	0.158	0.0780	<u>0.046</u>	0.060	0.228	0.035	0.050	<u>0.048</u>	0.198
	Mean	0.039	0.072	0.107	0.071	<u>0.042</u>	0.056	0.178	0.034	0.045	<u>0.044</u>	0.132
Electricity	0.125	0.070	<u>0.109</u>	0.181	0.712	0.289	0.417	0.434	0.043	<u>0.100</u>	0.120	0.213
	0.250	0.074	<u>0.123</u>	0.235	0.773	0.344	0.468	0.573	0.047	<u>0.102</u>	0.123	0.229
	0.375	0.078	<u>0.136</u>	0.317	0.837	0.405	0.528	0.755	0.050	<u>0.105</u>	0.122	0.244
	0.500	0.085	<u>0.151</u>	0.439	0.910	0.475	0.601	1.008	0.054	<u>0.107</u>	0.124	0.259
	Mean	0.077	<u>0.130</u>	0.293	0.808	0.378	0.504	0.693	0.049	<u>0.104</u>	0.122	0.236

Table 14: Full **Imputation Results (MSE, Lower is better)**: Hybrid Masking setup. Lowest MSE score is indicated in **Bold** and second lowest MSE score is Underlined

length 512. The datasets with fewer than 10 samples in a class are excluded. This results in a total of 5,960 indexed time-series segments.

Query Generation To construct the query sets, we apply stronger augmentations to the indexed samples to simulate real-world distortions and test the robustness of the learned embeddings. Specifically, each query is created by applying a combination of:

- within $\pm 20\%$ random time shift,
- within $\pm 20\%$ random scaling transformation, and
- Gaussian noise with standard deviation of 10% magnitude of the scaled time-series data.

This setup serves two purposes: (i) it evaluates whether embeddings are invariant to temporal misalignment and other distortions and (ii) it allows for automatic ground-truth labeling since each query is derived from a known indexed sample. The same augmentation strategy is applied to both the synthetic and real datasets, ensuring a consistent evaluation framework. These challenging augmentations make the retrieval task more realistic and better reflect practical use cases in time-series analysis.

Tasks We define two types of retrieval tasks to evaluate semantic similarity at different levels:

- **Family Match:** Measures coarse-grained retrieval—i.e., finding samples with the same high-level structure. For synthetic data, each of the 56 pattern combinations defines a class. For real data, each dataset name is treated as a class.

Dataset	MR	Zeroshot/Prompt_Tuned/Statistical							Finetuned/Supervised			
		TSPulse	UniTS (PMT)	MOMENT	Naive	Linear	Nearest	Cubic	TSPulse	Non-Stationary Transformer	TimesNet	FED-former
ETTh1	0.125	0.209	<u>0.239</u>	0.302	1.035	0.530	0.645	1.100	0.055	<u>0.115</u>	0.138	0.264
	0.250	0.225	<u>0.269</u>	0.355	1.092	0.633	0.760	1.819	0.070	<u>0.156</u>	0.157	0.377
	0.375	0.246	<u>0.299</u>	0.430	1.131	0.729	0.875	2.978	0.098	<u>0.192</u>	0.201	0.469
	0.500	0.272	<u>0.331</u>	0.518	1.165	0.816	0.987	5.101	0.129	<u>0.234</u>	0.263	0.554
	Mean	0.238	<u>0.284</u>	0.401	1.106	0.677	0.817	2.749	0.088	<u>0.174</u>	0.19	0.416
ETTh2	0.125	0.081	<u>0.150</u>	<u>0.105</u>	0.201	0.117	0.147	0.640	0.050	0.093	0.089	0.556
	0.250	0.088	<u>0.195</u>	<u>0.121</u>	0.218	0.132	0.163	0.997	0.055	0.109	<u>0.104</u>	0.948
	0.375	0.098	<u>0.250</u>	<u>0.142</u>	0.235	0.148	0.182	1.640	0.059	<u>0.121</u>	0.123	1.320
	0.500	0.113	<u>0.360</u>	<u>0.168</u>	0.255	<u>0.165</u>	0.202	2.871	0.068	<u>0.136</u>	0.140	1.673
	Mean	0.095	<u>0.239</u>	<u>0.134</u>	0.228	0.140	0.173	1.537	0.058	0.115	<u>0.114</u>	1.124
ETTm1	0.125	0.068	<u>0.137</u>	0.133	0.279	<u>0.088</u>	0.140	0.373	0.023	<u>0.047</u>	0.060	0.181
	0.250	0.081	<u>0.175</u>	0.179	0.369	<u>0.120</u>	0.181	0.595	0.028	<u>0.062</u>	0.082	0.280
	0.375	0.100	<u>0.206</u>	0.246	0.480	<u>0.170</u>	0.238	0.976	0.038	<u>0.085</u>	0.106	0.384
	0.500	0.128	<u>0.262</u>	0.339	0.620	<u>0.248</u>	0.325	1.732	0.052	<u>0.107</u>	0.146	0.493
	Mean	0.094	<u>0.195</u>	0.224	0.437	<u>0.157</u>	0.221	0.919	0.035	<u>0.076</u>	0.098	0.335
ETTm2	0.125	0.046	<u>0.099</u>	0.061	0.092	<u>0.051</u>	0.066	0.251	0.022	<u>0.041</u>	0.046	0.448
	0.250	0.050	<u>0.113</u>	0.072	0.104	<u>0.057</u>	0.074	0.393	0.027	<u>0.047</u>	0.057	0.712
	0.375	0.056	<u>0.138</u>	0.088	0.119	<u>0.065</u>	0.083	0.630	0.030	<u>0.055</u>	0.068	1.015
	0.500	0.065	<u>0.179</u>	0.108	0.139	<u>0.076</u>	0.096	1.094	0.039	<u>0.064</u>	0.070	1.404
	Mean	0.054	<u>0.132</u>	0.082	0.113	<u>0.062</u>	0.080	0.592	0.030	<u>0.052</u>	0.060	0.895
Weather	0.125	0.048	<u>0.065</u>	0.063	0.090	<u>0.053</u>	0.068	0.281	0.034	0.051	0.046	0.133
	0.250	0.053	<u>0.075</u>	0.072	0.099	<u>0.058</u>	0.074	0.447	0.038	0.056	<u>0.052</u>	0.197
	0.375	0.058	<u>0.081</u>	0.086	0.112	<u>0.065</u>	0.082	0.731	0.042	0.062	<u>0.057</u>	0.262
	0.500	0.066	<u>0.093</u>	0.103	0.128	<u>0.074</u>	0.093	1.219	0.047	0.073	<u>0.067</u>	0.324
	Mean	0.056	<u>0.078</u>	0.081	0.107	<u>0.062</u>	0.079	0.669	0.04	0.060	<u>0.056</u>	0.229
Electricity	0.125	0.084	<u>0.110</u>	0.159	1.257	0.571	0.718	1.018	0.053	<u>0.110</u>	0.121	0.238
	0.250	0.090	<u>0.121</u>	0.197	1.351	0.732	0.880	1.741	0.057	<u>0.114</u>	0.124	0.262
	0.375	0.100	<u>0.131</u>	0.264	1.416	0.878	1.050	2.924	0.062	<u>0.114</u>	0.128	0.283
	0.5	0.115	<u>0.141</u>	0.388	1.46	1.005	1.212	5.008	0.068	<u>0.118</u>	0.131	0.302
	Mean	0.097	<u>0.126</u>	0.252	1.371	0.797	0.965	2.673	0.060	<u>0.114</u>	0.126	0.271

Table 15: Full Imputation Results (MSE, Lower is better): Block-wise masking setup. Lowest MSE score is indicated in **Bold** and second lowest MSE score is Underlined

Model Variant	MSE (\downarrow)	IMP (%)
Irregular Hybrid Masking Eval		
TSPulse	0.074	
w/o Dual-Space	0.081	8% \downarrow
w/o Hybrid Pretraining	0.354	79% \downarrow
Regular Block Masking Eval		
TSPulse	0.106	
w/o Dual-Space	0.115	8% \downarrow
w/o Hybrid Pretraining	0.098	7.5% \uparrow

Table 16: Imputation–Ablation Study Summary, MSE, Lower is better. Detailed results in Table 17

- **Fine-Grained Match:** Measures fine-grained retrieval—i.e., In synthetic data, each pattern-frequency combination ($56 \times 10 = 560$) is treated as a class. In real data, each (dataset name, class index) pair defines a unique class, totaling 596.

Implementation & Evaluation Metrics We compute semantic similarity using Euclidean distance between embeddings from the pre-trained models. We use the *Faiss* library [6] to index embeddings. Performance is evaluated using standard retrieval metrics applied to the top-3 retrieved candidates:

- **PREC@3:** Precision at top-3.
- **MRR@3:** Mean Reciprocal Rank at top-3.
- **AP@3:** Average Precision at top-3.

Dataset	Block_Masking			Hybrid_Masking		
	TSPulse w/o Dual-Space	TSPulse	TSPulse w/o Hybrid Pre-training	TSPulse w/o Dual-Space	TSPulse	TSPulse w/o Hybrid Pre-training
ETTh1	0.251	<u>0.238</u>	0.220	<u>0.173</u>	0.163	0.539
ETTh2	0.099	<u>0.095</u>	0.091	<u>0.074</u>	0.070	0.231
ETTh1	0.105	<u>0.094</u>	0.088	<u>0.063</u>	0.057	0.485
ETTh2	0.056	<u>0.054</u>	0.053	<u>0.039</u>	0.037	0.163
Weather	0.058	<u>0.056</u>	0.055	<u>0.041</u>	0.039	0.155
Electricity	0.120	<u>0.097</u>	0.083	<u>0.094</u>	0.077	0.552
Mean	0.115	<u>0.106</u>	0.098	<u>0.081</u>	0.074	0.354

Table 17: **Imputation Result (MSE, Lower is better)**: Block and Hybrid masking setup averaged across all 4 different mask ratios for different variants of TSPulse. Lowest MSE score across variants is highlighted in **Bold** and second lowest MSE score is Underlined. More Detailed results in Table 18.

Dataset	Mask_Ratio	Block Masking			Hybrid Masking		
		TSPulse w/o Dual_space	TSPulse	TSPulse w/o Hybrid Pre-training	TSPulse w/o Dual_space	TSPulse	TSPulse w/o Hybrid Pre-training
ETTh1	0.125	0.227	<u>0.209</u>	0.189	<u>0.158</u>	0.146	0.498
	0.250	0.241	<u>0.225</u>	0.208	<u>0.166</u>	0.155	0.528
	0.375	0.258	<u>0.246</u>	0.230	<u>0.177</u>	0.168	0.553
	0.500	0.279	<u>0.272</u>	0.255	<u>0.190</u>	0.183	0.578
	Mean	0.251	<u>0.238</u>	0.220	<u>0.173</u>	0.163	0.539
ETTh2	0.125	0.086	<u>0.081</u>	0.077	<u>0.069</u>	0.065	0.216
	0.250	0.093	<u>0.088</u>	0.084	<u>0.072</u>	0.068	0.226
	0.375	0.102	<u>0.098</u>	0.094	<u>0.075</u>	0.072	0.235
	0.500	0.115	<u>0.113</u>	0.107	<u>0.080</u>	0.077	0.247
	Mean	0.099	<u>0.095</u>	0.091	<u>0.074</u>	0.070	0.231
ETTh1	0.125	0.078	<u>0.068</u>	0.065	<u>0.055</u>	0.049	0.449
	0.250	0.091	<u>0.081</u>	0.076	<u>0.060</u>	0.053	0.470
	0.375	0.110	<u>0.100</u>	0.093	<u>0.065</u>	0.058	0.496
	0.500	0.139	<u>0.128</u>	0.119	<u>0.072</u>	0.066	0.526
	Mean	0.105	<u>0.094</u>	0.088	<u>0.063</u>	0.057	0.485
ETTh2	0.125	0.048	<u>0.046</u>	0.044	<u>0.036</u>	0.034	0.154
	0.250	0.052	<u>0.050</u>	0.049	<u>0.037</u>	0.036	0.159
	0.375	0.058	<u>0.056</u>	0.055	<u>0.040</u>	0.038	0.166
	0.500	0.067	<u>0.065</u>	0.063	<u>0.042</u>	0.041	0.174
	Mean	0.056	<u>0.054</u>	0.053	<u>0.039</u>	0.037	0.163
Weather	0.125	<u>0.051</u>	0.048	0.048	<u>0.038</u>	0.036	0.146
	0.250	0.055	<u>0.053</u>	0.051	<u>0.039</u>	0.038	0.151
	0.375	0.060	<u>0.058</u>	0.057	<u>0.042</u>	0.040	0.157
	0.500	0.067	<u>0.066</u>	0.063	<u>0.044</u>	0.042	0.165
	Mean	0.058	<u>0.056</u>	0.055	<u>0.041</u>	0.039	0.155
Electricity	0.125	0.105	<u>0.084</u>	0.069	<u>0.085</u>	0.070	0.488
	0.250	0.113	<u>0.090</u>	0.076	<u>0.090</u>	0.074	0.539
	0.375	0.124	<u>0.100</u>	0.086	<u>0.096</u>	0.078	0.575
	0.500	0.138	<u>0.115</u>	0.102	<u>0.104</u>	0.085	0.607
	Mean	0.120	<u>0.097</u>	0.083	<u>0.094</u>	0.077	0.552

Table 18: Full **Imputation Results (MSE, Lower is better)**: Comparison of three variants of TSPulse (a) **TSPulse w/o Dual_Space** : TSPulse model only pre-trained with time domain input (b) **TSPulse** : TSPulse model pre-trained with both time and frequency patches (c) **TSPulse w/o Hybrid_Masking** : TSPulse model pre-trained with block masking

- **NDCG@3**: Normalized Discounted Cumulative Gain at top-3.

We evaluate the inference time of each model. Specifically, we set the batch size to 1,024 and accumulate the forward computation time of the model over the dataset. The measured computation time is divided by the size of the dataset to derive the per-sample computation time.

Results Figure 7 presents a comparative evaluation of TSPulse’s similarity search performance against the zero-shot embeddings produced by two recent pre-trained models: MOMENT and Chronos. To ensure a fair and resource-efficient comparison, we use their smallest available variants, aligning closely with TSPulse in embedding dimensionality and enabling comparable indexing throughput.

As shown in the figure, TSPulse consistently outperforms both baselines across retrieval tasks. For the **Family Match** task, which assesses the model’s ability to retrieve semantically similar patterns,

Dataset	Mask_Ratio	MOMENT		UniTS_PMT	
		Heterogenous	Only_Zeros	Heterogenous	Only_Zeros
ETTh1	0.125	<u>0.324</u>	0.315	0.220	0.220
	0.250	0.387	<u>0.391</u>	<u>0.251</u>	0.250
	0.375	0.468	<u>0.487</u>	<u>0.288</u>	0.287
	0.500	0.568	<u>0.599</u>	<u>0.322</u>	0.319
	Mean	0.437	<u>0.448</u>	<u>0.27</u>	0.269
ETTh2	0.125	0.132	<u>0.256</u>	0.150	<u>0.151</u>
	0.250	0.202	<u>0.441</u>	<u>0.211</u>	0.199
	0.375	0.332	<u>0.649</u>	<u>0.326</u>	0.300
	0.500	0.542	<u>0.939</u>	<u>0.371</u>	0.364
	Mean	0.302	<u>0.571</u>	<u>0.264</u>	0.254
ETTm1	0.125	0.156	<u>0.173</u>	0.123	0.123
	0.250	0.218	<u>0.251</u>	0.156	0.156
	0.375	0.299	<u>0.344</u>	0.187	0.187
	0.500	0.407	<u>0.462</u>	<u>0.226</u>	0.222
	Mean	0.270	<u>0.308</u>	<u>0.173</u>	0.172
ETTm2	0.125	0.085	<u>0.217</u>	0.096	0.096
	0.250	0.149	<u>0.405</u>	<u>0.096</u>	0.092
	0.375	0.272	<u>0.605</u>	<u>0.136</u>	0.126
	0.500	0.48	<u>0.895</u>	<u>0.186</u>	0.172
	Mean	0.247	<u>0.530</u>	<u>0.129</u>	0.122
Weather	0.125	0.069	<u>0.090</u>	0.059	0.059
	0.25	0.086	<u>0.124</u>	0.070	0.070
	0.375	0.115	<u>0.166</u>	<u>0.075</u>	0.074
	0.500	0.158	<u>0.223</u>	<u>0.087</u>	0.085
	Mean	0.107	<u>0.151</u>	<u>0.073</u>	0.072
Electricity	0.125	0.181	<u>0.189</u>	<u>0.110</u>	0.109
	0.250	0.235	<u>0.252</u>	<u>0.124</u>	0.123
	0.375	0.317	<u>0.344</u>	<u>0.137</u>	0.136
	0.500	0.439	<u>0.472</u>	<u>0.153</u>	0.151
	Mean	0.293	<u>0.314</u>	<u>0.131</u>	0.130

Table 19: Full **Imputation Results (MSE, Lower is better)**: MOMENT & UniTS_PMT in **hybrid** setup. Heterogenous : Used the learned mask token to replace the fully missing patches and zeros at other missing positions, Only_Zeros : Using zeros as input to the model at every missing position.

TSPulse achieves over 25% higher accuracy than MOMENT. In the more challenging **Fine-Grained Match** task, which requires precise pattern localization, TSPulse demonstrates a 40% performance gain over MOMENT. TSPulse also outperforms Chronos by +100% in both settings.

In addition to accuracy gains, TSPulse also offers substantial efficiency benefits. Its embeddings are $2\times$ smaller than those of MOMENT and Chronos, leading to faster search and reduced memory overhead. In deployment benchmarks, TSPulse enables $10\text{--}100\times$ faster inference on CPU and $9\text{--}15\times$ faster inference on GPU, owing to its lightweight architecture and low memory footprint. Importantly, TSPulse achieves these results while being over $40\times$ smaller in model size, making it highly suitable for real-time, resource-constrained environments.

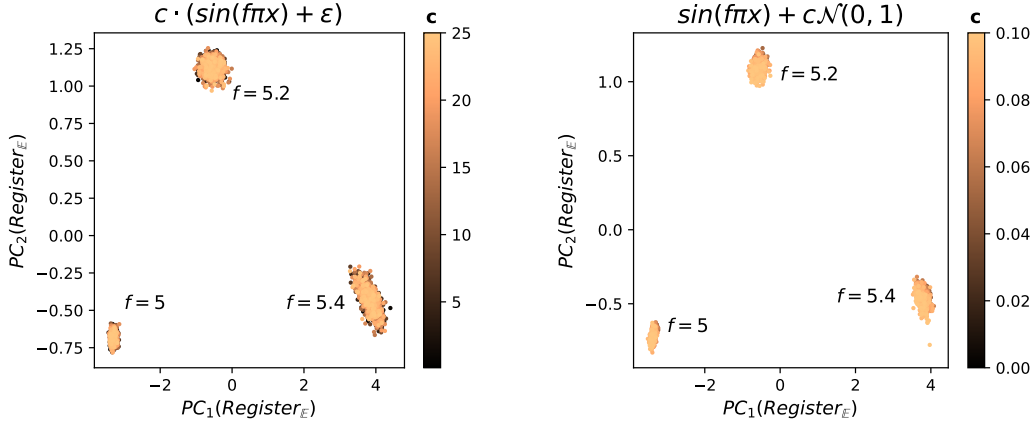
Tables 21 and 22 summarize the scores of PREC@3, AP@3, NDCG@3, and MRR@3. The average scores in Table 21 are plotted in Figure 7.

Robustness to Augmentation Complexity To further evaluate the robustness of pre-trained models in the similarity search task, we systematically vary the intensity of augmentations used to generate the query samples. Specifically, we introduce a scaling factor $s \in \{0, 10, 20, 30, 40, 50\}$, which controls the strength of three types of distortions: time shifts, magnitude scaling, and additive noise. For example, when $s = 10$, a 10% random temporal shift, 10% scaling perturbation, and 10% additive Gaussian noise are applied to each query. The noise level is capped at 10% across all values of s to maintain a realistic noise regime, as extreme noise rarely dominates in practical time-series settings.

The motivation behind increasing s lies in simulating more challenging retrieval scenarios. In time-series data, even small time shifts or scaling changes can result in significantly different signal appearances, despite underlying similarity in semantics. By gradually increasing s , we create a

controlled framework to stress-test the distortion invariance of learned embeddings. The setting where $s = 0$ corresponds to a sanity check: since the query is identical to an indexed sample, a high retrieval score is expected from any well-trained model.

Figure 14 presents the retrieval performance of TSPulse, MOMENT, and Chronos across different augmentation levels. As expected, all models perform well at $s = 0$, but performance declines with increasing augmentation strength. Notably, TSPulse exhibits significantly greater resilience, maintaining higher scores across all values of s . Compared to MOMENT and Chronos, the performance of TSPulse degrades more slowly, demonstrating superior robustness to distortions in temporal alignment, signal scaling, and additive noise. These results highlight the effectiveness of TSPulse’s hybrid masking pre-training and register-token embeddings in capturing stable, semantically meaningful representations under realistic, noisy retrieval conditions.



(a) **Sensitivity to Magnitude Scaling:** PCA of register embeddings with three distinct frequency groups, colored by amplitude scale factor (c). The embeddings remain compact across scale variations.

(b) **Sensitivity to Noise:** PCA of register embeddings for noisy sine waves with three distinct frequency groups, colored by noise factor (c). Embedding variation due to noise is small compared to frequency-induced separation.

Figure 9: Scatter plots of the first two PCA components of *TSPulse* register embeddings under (a) amplitude scaling and (b) additive Gaussian noise. Each setup contains three distinct frequency-based groups ($f = \{5, 5.2, 5.4\}$). The colour in the scatter plot indicates the value of the variable c as indicated by the corresponding equation.

A.12 Sensitivity analysis of *TSPulse* Short Register embeddings

In this section, we study the behavior of the short register embeddings—i.e., zero-shot semantic embeddings—learned by *TSPulse*. These embeddings are designed to capture compact, meaningful representations of time-series patterns and are primarily used for retrieval and semantic similarity tasks. We perform a detailed sensitivity analysis to understand how these embeddings respond when various properties of the input data are altered, including magnitude changes, added noise, missing values, time-shifts (i.e., phase variations), and changes in frequency and patterns.

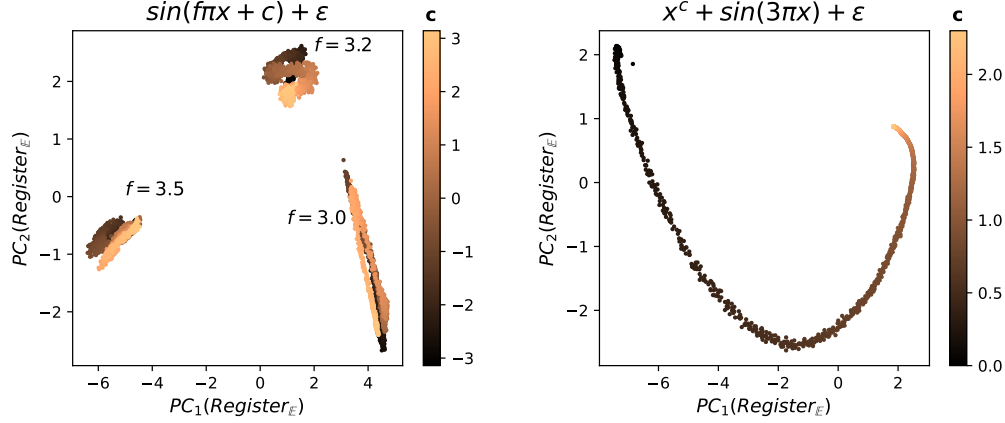
Ideally, we want the embeddings to remain invariant to factors such as noise, magnitude scaling, missing values, and temporal misalignments, while being highly responsive to core semantic characteristics like frequency patterns (e.g., periodicity, seasonality) and distinctive shape structures in the data. Such behavior ensures robust semantic retrieval—retrieving similar patterns despite distortions—while preserving the ability to distinguish fundamentally different signal classes.

Sensitivity to magnitude scaling To assess whether the register embeddings capture only semantically meaningful variations, we analyze their sensitivity to magnitude/amplitude scaling and compare it against their responses to frequency shifts. Frequency shift directly influences the structural semantics of time-series signals—such as periodicity—whereas magnitude scale changes are often irrelevant. This contrast allows us to quantify and appreciate the embedding’s robustness to irrelevant perturbations. We generate a synthetic dataset using sinusoidal signals with three distinct frequencies,

and we apply a linear amplitude scaling factor c , sampled uniformly from the range $[1, 25]$. We then extract register embeddings for each scaled variant and analyze their variation in the embedding space.

Our results in Figure 9a show that while register embeddings vary noticeably across different frequencies, they remain very stable under magnitude scaling. For this analysis, we extract the *TSPulse* register embedding for each data point, along with its associated scaling factor and frequency label. PCA projections reveal that the intra-cluster variation caused by amplitude scaling is small compared to the inter-cluster separation induced by frequency differences. This indicates that the embeddings are largely invariant to amplitude, an essential property for semantic retrieval tasks, where magnitude often varies due to normalization, sensor artifacts, or contextual shifts. By maintaining sensitivity to core signal properties such as frequency while suppressing irrelevant variations like scale, the model yields robust and meaningful representations suitable for retrieval.

Sensitivity to noise We evaluate the impact of additive noise on the register embeddings by analyzing how noise-induced variations compare to those caused by changes in frequency. Synthetic sine wave signals are generated with distinct frequency groups, and Gaussian noise is added to simulate varying signal-to-noise ratios. Embeddings are extracted for each noisy signal, and their spatial variation is analyzed using intra-group and inter-group distances. Intra-group variation reflects sensitivity to noise, while inter-group separation captures the embedding’s response to frequency changes. As shown in Figures 9b, the impact of noise on the embeddings is minimal compared to the clear separation observed across different frequencies. This highlights the robustness of *TSPulse* embeddings to noise—an essential property for maintaining semantic consistency in real-world applications where signal degradation to noise is common.



(a) **Sensitivity to Phase Shifts:** PCA projections of the register embeddings of phase shifted instances with three distinct frequencies. (b) **Sensitivity to Trends:** PCA projections of the register embeddings of the data with varying trend.

Figure 10: Data patterns in register embedding space. The colour in the scatter plot indicates the value of the variable c as indicated by the corresponding equation. The control experiment reveals, register embeddings are strongly sensitive to data trend and frequency and relatively less sensitive to phase (time shift).

Sensitivity to time shifts (phase variations) To assess the sensitivity of register embeddings to phase (i.e. time-shift) variations, we conduct a control experiment using synthetic signals of the form $\sin(f\pi x + c) + \epsilon$, where $f \in \{3, 3.2, 3.5\}$ represents the frequency, c denotes the phase shift (i.e., time-shift), and ϵ is Gaussian noise. We change the phase c continuously from $-\pi$ to π to simulate temporal misalignments commonly seen in real-world indexed data.

This setup emulates practical scenarios in semantic time-series search, where the same underlying pattern may be indexed at different time offsets in a database. In such cases, time shift invariant embeddings enable robust retrieval, ensuring semantically similar signals are matched even with minor time shifts. Conversely, sensitivity to frequency is desirable, as frequency often encodes core

data characteristics such as seasonality or periodic structure. Thus, being able to distinguish small frequency differences allows the model to separate fundamentally different patterns more effectively.

PCA on register embeddings shows variations in frequency lead to significantly larger shifts in the embedding space compared to phase changes. The first two PCA components reveal tight, well-separated clusters corresponding to each frequency, while phase shifts produce only minor within-cluster variation (Figure 10a). This confirms that the embeddings are relatively less sensitive to phase shifts while remaining distinctly responsive to frequency variations – an ideal characteristic for robust semantic search.

Sensitivity to data trend Here, we investigate how the register embedding models data trends. To carry out the control experiment with synthetic data with functional form $x^c + \sin(3\pi x) + \epsilon$. By varying the variable c , we generate different monotonic trend patterns in the data. We continuously varied the data trend parameter (c) from 0 to 2.5. Where 0 means no data trend, while 2.0 represents a quadratic pattern in the input data. The PCA analysis of the register embeddings shows that it distinctly models the monotonic data trend.

Sensitivity to shape space In these experiments, we analyse the sensitivity of the embedding space to changes in the function shape, compared to frequency and phase change. For these experiment we use three distinct data generating functions, of the form $\mathbb{F}_1(x) = \sin(x)$, $\mathbb{F}_2 = 2 * (\sin(x) + 1)^4 - 1$, and $\mathbb{F}_3 = 2 * \sqrt[4]{\sin(x) + 1} - 1$ (Figure 11). Each of these functions is periodic and trigonometric. We generate a dataset using these three generating functions. For each generating function, we sample data with three distinct frequency groups $f = \{5, 5.2, 5.4\}$, for each frequency we generate synthetic data by randomly sampling phase between $(-\pi, \pi)$. We carry out PCA analysis on the register embedding of this dataset (Figure 12). The analysis reveals the frequency groups form distinct clusters. Frequency clusters from same generating function are closer compared to clusters from different generating function.

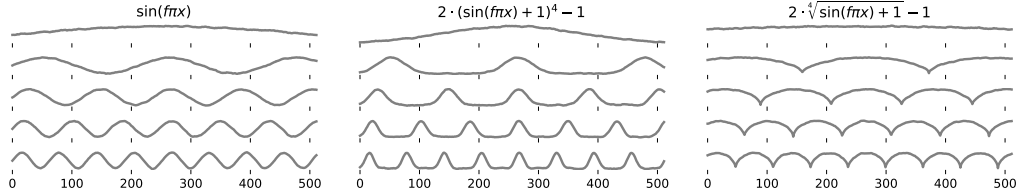


Figure 11: Data generated from the three synthetic data generator functions with varying frequencies.

Sensitivity to missing values To assess the robustness of register embeddings to missing data, we generate synthetic signals using the function $\sin(c\pi x)$, where the frequency parameter c is uniformly sampled from the range $[1, 15]$. Missing values are simulated by applying block masks of fixed patch length ($pl = 8$) to the input sequence, and we vary the mask ratio to control the extent of missingness.

We extract register embeddings under different masking levels and project them using PCA. As shown in Figure 13, the embedding space remains highly stable and preserves the underlying frequency-based structure even when up to 35% of the input data missingness. Distortion in the embedding manifold is observed only at very high mask ratios, where a majority of the signal is occluded. These results demonstrate that *TSPulse* embeddings are very robust to moderate levels of missing data—a valuable property in real-world time-series applications where sensor dropouts and irregular sampling are common.

A.13 Runtime Computational Analysis of TSPulse and other Pre-trained models

In this section we do the computational analysis of TSPulse with all the other pre-trained models that are used for benchmarking across different tasks in this work. These models include MOMENT [15], VQShape [35], Chronos [1], TimesFM [5] and Lag-llama [27]. We are skipping UniTS [13] from this exercise because the total size of UniTS prompt tuned models vary significantly depending on the multi-task setting it has been trained for; for instance, the prompt tuned model used in our

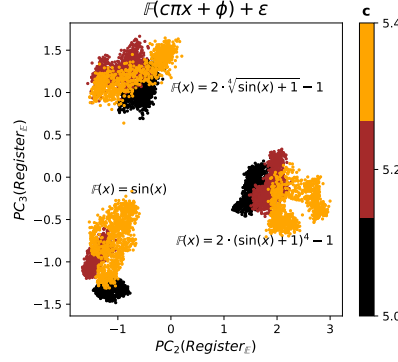


Figure 12: **Sensitivity to shape:** Cluster analysis of the register embedding of the data with three distinct function class. The cluster corresponding to the respective generator function is annotated in the figure. The colour represents the frequency associated with the data point (c). The strong separation between the embeddings of the data instances from different generator functions indicates that register embedding distinguishes the data instances by their shapes.

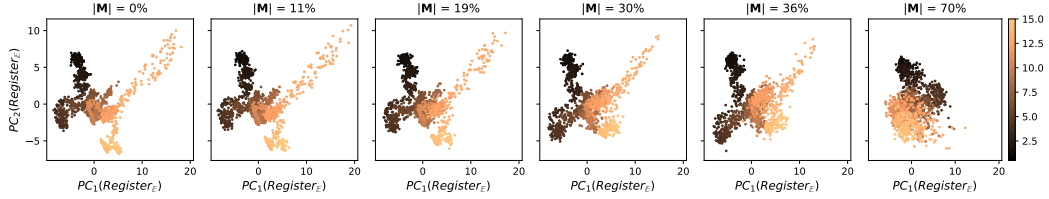


Figure 13: **Sensitivity to missing values:** First two principal components computed of the register embeddings, with varying mask ratio applied to the input data. The colour indicates the frequency of the synthetic data point. The plot indicates register embedding is fairly robust to missing data.

benchmarking for classification has 10M parameters but the model prompt tuned for the imputation task has only 4M parameters.

In this analysis, we demonstrate the suitability of TSPulse for rapid time-series analysis by highlighting its computational advantages over larger pre-trained models. With only 1M parameters, TSPulse offers significant efficiency benefits in terms of per-batch CPU inference time, GPU inference time, and peak GPU memory usage. These comparisons are made against all pre-trained baselines discussed above. Refer to Table 23 for detailed results.

All computational analysis experiments were conducted on a system equipped with an NVIDIA A100 GPU (80GB), 16 CPU cores, and 256GB of RAM. For inference time and peak memory usage measurements, a zero tensor input of shape (batch size = 32, sequence length = 512, channels = 5) was used.

A.14 Limitations and Future work

While TSPulse demonstrates strong performance across a range of tasks, including similarity search, classification, anomaly detection, and imputation, there are several important areas for future development. One key direction is expanding its application to more downstream use cases, such as regression and full-fledged forecasting, to further extend its versatility. Additionally, TSPulse can be adapted for more challenging few-shot learning scenarios, particularly in classification tasks with limited labeled data. This would allow the model to perform effectively even in situations where labeled data is scarce, a common challenge in many real-world applications.

Another exciting direction is the expansion of TSPulse’s capabilities by infusing semantic search with anomaly detection. By leveraging its powerful embeddings, future work could focus on identifying similar anomaly patterns from historical time-series data and retrieving related solutions from associated ticketing systems or knowledge bases. This would enhance its application in anomaly

Base pattern name	Base pattern equation
sin	$x_t = \sin(b_t)$
modcos	$x_t = \cos(b_t) \cdot \sin(b_t/2)$
square-modcos	$x_t = \text{sign}(\sin(b_t)) \cdot \cos(2b_t) $
gaussian-spike	$x_t = \exp(-40(c_t - f/2)^2)$
impulse	$x_t = \begin{cases} 1 & \text{if } \text{mod}(t, 10f) = 0 \\ 0 & \text{otherwise} \end{cases}$
randwalk	$x_t = f + \sum_{t'=0}^t \varepsilon_{t'}$
sincos	$x_t = \sin(b_t) \cdot \cos(2 * b_t)$
tanhmix	$x_t = \tanh(\sin(3 * b_t)) + 0.2\varepsilon_t$

Table 20: Eight base patterns for synthetic data. $b_t = 2\pi tf/512$, $t = 0, 1, \dots, 511$, sign is the sign function, ε is drawn from the standard Gaussian distribution, i.e., $\varepsilon \sim N(0, 1)$, and mod is the modulo operation.

	Family match						Fine-grained match					
	PREC@3			MRR@3			PREC@3			MRR@3		
	TSPulse	MOMENT	Chronos	T	M	C	T	M	C	T	M	C
Real	0.645	0.389	0.116	0.856	0.491	0.144	0.474	0.216	0.057	0.750	0.335	0.087
Synth.	0.711	0.674	0.352	0.713	0.679	0.361	0.695	0.615	0.295	0.697	0.619	0.304
Avg.	0.678	0.532	0.234	0.784	0.585	0.252	0.584	0.415	0.176	0.723	0.477	0.195

Table 21: **Similarity Search.** PREC@3 and MRR@3 on Synthetic and Real data. Higher is better.

detection and make TSPulse a valuable tool for problem resolution across various industries, such as IT operations and healthcare. Additionally, exploring multi-modal fusion of TSPulse embeddings with those from other data types like text and images could unlock cross-domain applications, enabling more sophisticated models for complex tasks.

Finally, while TSPulse is lightweight and efficient, there is potential to enhance its ability to perform continuous learning. In dynamic environments where new data is constantly being generated, it is crucial to update the pre-trained model with new information while ensuring that previously learned knowledge is preserved. Future work will focus on implementing incremental learning techniques, enabling TSPulse to adapt to new data without forgetting the patterns learned from prior training. This approach will make TSPulse even more robust for real-time applications, where the model can continuously improve over time, maintaining both accuracy and stability across evolving datasets.

	Family match						Fine-grained match					
	AP@3			NDCG@3			AP@3			NDCG@3		
	TSPulse	MOMENT	Chronos	T	M	C	T	M	C	T	M	C
Real	0.619	0.366	0.105	0.683	0.403	0.118	0.447	0.195	0.050	0.525	0.234	0.061
Synth.	0.710	0.672	0.348	0.711	0.675	0.353	0.694	0.613	0.290	0.695	0.615	0.295
Avg.	0.664	0.519	0.226	0.697	0.539	0.235	0.570	0.404	0.170	0.610	0.425	0.178

Table 22: **Similarity Search.** AP@3 and NDCG@3 on Synthetic and Real data. Higher is better.

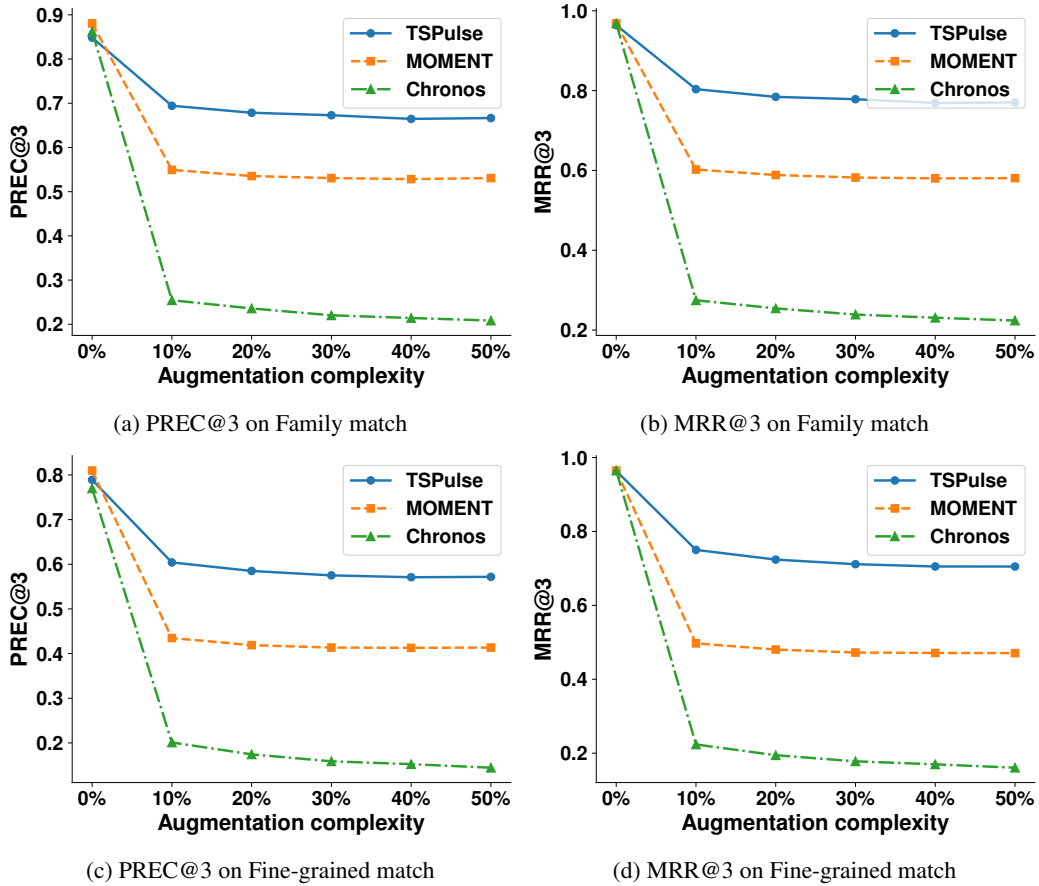


Figure 14: TSPulse Similarity Search Ablation Study

Model	Params (M)	GPU Inference Time (ms)	CPU Inference Time (s)	Max. Memory (GB)
TSPulse	1.06	7.16	0.06	0.39
MOMENT (small)	35.34 (33.3X)	32.57 (4.5X)	2.74 (45.7X)	0.56 (1.4X)
MOMENT (base)	109.64 (103.4X)	120.27 (16.8X)	7.60 (126.7X)	1.15 (2.9X)
MOMENT (large)	341.24 (321.9X)	405.42 (56.6X)	21.98 (366.3X)	2.30 (5.9X)
VQShape	37.09 (35.0X)	65.37 (9.1X)	1.15 (19.2X)	6.88 (17.6X)
Lag-llama	2.45 (2.3X)	236.00 (33.0X)	0.24 (4.0X)	1.01 (2.6X)
TimesFM	203.57 (192.0X)	101.80 (14.2X)	1.14 (19.0X)	0.87 (2.2X)
CHRONOS (tiny)	8.39 (7.9X)	39.81 (5.6X)	66.15 (1102.5X)	2.91 (7.5X)
CHRONOS (small)	46.15 (43.5X)	112.62 (15.7X)	201.62 (3360.3X)	5.86 (15.0X)
CHRONOS (base)	201.37 (190.0X)	328.37 (45.9X)	642.38 (10706.3X)	8.97 (23.0X)
CHRONOS (large)	708.96 (668.8X)	897.86 (125.4X)	1754.87 (29247.8X)	12.80 (32.8X)

Table 23: **Computational Analysis** of TSPulse and other pre-trained models. Per batch GPU inference time in milli-seconds(ms), CPU inference time in seconds(s), Maximum memory usage in GB and Number of parameters in millions(M) are reported. Lower is better.